J|A|C|S
ARTICLES
Published on Web 08/05/2006

Synthetic, Electrochemical, and Theoretical Studies of Tetrairidium Clusters Bearing Mono- and Bis[60]fullerene Ligands

Bo Keun Park,[†] Gaehang Lee,[†] Kyoung Hoon Kim,[‡] Hongkyu Kang,[†] Chang Yeon Lee,[†] Md. Arzu Miah,[†] Jaehoon Jung,[‡] Young-Kyu Han,*[,‡] and Joon T. Park*[,†]

Contribution from the Department of Chemistry and School of Molecular Science (BK 21), Korea Advanced Institute of Science and Technology (KAIST), Daejeon, 305-701, Korea, and Computational Chemistry Laboratory, Advanced Materials R&D, LG Chem, Ltd. Research Park, Daejeon, 305-380, Korea

Received March 16, 2006; E-mail: joontpark@kaist.ac.kr.; ykhan@lgchem.com

Abstract: Heating a mixture of $Ir_4(CO)_9(PPh_3)_3$ (**1**) and 2 equiv of C_{60} in refluxing chlorobenzene (CB) affords a "butterfly" tetrairidium−C_{60} complex $Ir_4(CO)_6\{\mu_3\text{-}\kappa^3\text{-}PPh_2(o\text{-}C_6H_4)P(o\text{-}C_6H_4)PPh(\eta^1\text{-}o\text{-}C_6H_4)\}(\mu_3\text{-}\eta^2\text{:}\eta^2\text{:}\eta^2\text{-}C_{60})$ (**3**, 36%). Brief thermolysis of **1** in refluxing chlorobenzene (CB) gives a "butterfly" complex $Ir_4(CO)_8\{\mu\text{-}k^2\text{-}PPh_2(o\text{-}C_6H_4)PPh\}\{\mu_3\text{-}PPh_2(\eta^1\text{:}\eta^2\text{-}o\text{-}C_6H_4)\}$ (**2**, 64%) that is both ortho-phosphorylated and ortho-metalated. Interestingly, reaction of **2** with 2 equiv of C_{60} in refluxing CB produces **3** (41%) by C_{60}-assisted ortho-phosphorylation, indicating that **2** is the reaction intermediate for the final product **3**. On the other hand, reaction of $Ir_4(CO)_8(PMe_3)_4$ (**4**) with excess (4 equiv) C_{60} in refluxing 1,2-dichlorobenzene, followed by treatment with $CNCH_2Ph$ at 70 °C, affords a square-planar complex with two C_{60} ligands and a face-capping methylidyne ligand, $Ir_4(CO)_3(\mu_4\text{-}CH)(PMe_3)_2(\mu\text{-}PMe_2)(CNCH_2Ph)(\mu\text{-}\eta^2\text{:}\eta^2\text{-}C_{60})(\mu_4\text{-}\eta^1\text{:}\eta^1\text{:}\eta^2\text{:}\eta^2\text{-}C_{60})$ (**5**, 13%) as the major product. Compounds **2**, **3**, and **5** have been characterized by spectroscopic and microanalytical methods, as well as by single-crystal X-ray diffraction studies. Cyclic voltammetry has been used to examine the electrochemical properties of **2**, **3**, **5**, and a related known "butterfly" complex $Ir_4(CO)_6(\mu\text{-}CO)\{\mu_3\text{-}k^2\text{-}PPh_2(o\text{-}C_6H_4)P(\eta^1\text{-}o\text{-}C_6H_4)\}(\mu_3\text{-}\eta^2\text{:}\eta^2\text{:}\eta^2\text{-}C_{60})$ (**6**). These cyclic voltammetry data suggest that a C_{60}-mediated electron transfer to the iridium cluster center takes place for the species $\mathbf{3}^{3-}$ and $\mathbf{6}^{2-}$ in compounds **3** and **6**. The cyclic voltammogram of **5** exhibits six well-separated reversible, one-electron redox waves due to the strong electronic communication between two C_{60} cages through a tetrairidium metal cluster spacer. The electrochemical properties of **3**, **5**, and **6** have been rationalized by molecular orbital calculations using density functional theory and by charge distribution studies employing the Mulliken and Hirshfeld population analyses.

Introduction

Considerable research efforts have been devoted to [60]-fullerene (C_{60}), the most abundant representative of the fullerene family, due to its potential application in materials science such as optical, magnetic, electronic, catalytic, and biological fields.[1] In recent years, seminal results with C_{60} research have been achieved in various areas of light emitting diodes,[2a] nonlinear optics,[2b] organic ferromagnets,[2c] superconductors,[2d] photovoltaic cells,[2e] nitrogen fixation,[2f] and interaction with biological targets.[2g,h] In particular, we have been interested in C_{60}−metal cluster exohedral metallofullerene complexes in order to investigate and understand the effects of metal cluster coordination on the chemical and physical properties of C_{60}, reactivities and electrochemical properties of these complexes, and ultimately to develop new electronic nanomaterials and nanodevices.[3]

Metal clusters can potentially accommodate all the known C_{60} π-bonding modes such as η^2-,[4] $\mu\text{-}\eta^2\text{:}\eta^2$-,[5] and η^5-types,[6] but the interaction of C_{60} with cluster framework has been dominated by the face-capping cyclohexatriene-like, $\mu_3\text{-}\eta^2\text{:}\eta^2\text{:}\eta^2\text{-}C_{60}$, bonding mode.[3a] The C_{60}−metal cluster complexes with

[†] Korea Advanced Institute of Science and Technology (KAIST).
[‡] LG Chem, Ltd. Research Park.

(1) (a) Mirkin, C. A.; Caldwell, W. B. *Tetrahedron*, **1996**, *52*, 5113−5130. (b) Wray, J. E.; Liu, K. C.; Chen, C. H.; Garrett, W. R.; Payne, M. G.; Goedert, R.; Templeton, D. *Appl. Phys. Lett.* **1994**, *64*, 2785−2787. (c) Jensen, A. W.; Wilson, S. R.; Schuster, D. I. *Bioorg. Med. Chem.* **1996**, *4*, 767−779.

(2) (a) Hutchison, K.; Gao, J.; Schick, G.; Rubin, Y.; Wudl, F. *J. Am. Chem. Soc.* **1999**, *121*, 5611−5612. (b) Kuang, L.; Chen, Q.; Sargent, E. H.; Wang, Z. Y. *J. Am. Chem. Soc.* **2003**, *125*, 13648−13649. (c) Makarova, T. L.; Sundqvist, B.; Höhne, R.; Esquinazi, P.; Kopelevich, Y.; Scharff, P.; Davydov, V. A.; Kashevarova, L. S.; Rakhmanina, A. V. *Nature* **2001**, *413*, 716−718. (d) Margadonna, S.; Aslanis, E.; Prassides, K. *J. Am. Chem. Soc.* **2002**, *124*, 10146−10156. (e) Hasobe, T.; Imahori, H.; Kamat, P. V.; Ahn, T. K.; Kim, S. K.; Kim, D.; Fujimoto, A.; Hirakawa, T.; Fukuzumi, S. *J. Am. Chem. Soc.* **2005**, *127*, 1216−1228. (f) Nishibayashi, Y.; Saito, M.; Uemura, S.; Takekuma, S.-i.; Takekuma, H.; Yoshida, Z.-i. *Nature* **2004**, *428*, 279−280. (g) Nakamura, E.; Isobe, H. *Acc. Chem. Res.* **2003**, *36*, 807−815. (h) Bolskar, R. D.; Benedetto, A. F.; Husebo, L. O.; Price, R. E.; Jackson, E. F.; Wallace, S.; Wilson, L. J.; Alford, J. M. *J. Am. Chem. Soc.* **2003**, *125*, 5471−5478.

(3) (a) Lee, K.; Song, H.; Park, J. T. *Acc. Chem. Res.* **2003**, *36*, 78−86 and references therein. (b) Balch, A. L.; Olmstead, M. M. *Chem. Rev.* **1998**, *98*, 2123−2165. (c) Stephens, A.; Green, M. L. H. *Adv. Inorg. Chem.* **1997**, *44*, 1−43.

10.1021/ja0616027 CCC: $33.50

this relatively strong bonding mode exhibited remarkable thermal and electrochemical stabilities, uniquely suitable for various device applications[3a] in contrast to other previously known C_{60}−metal complexes. We have been interested in the conversion of the existing C_{60} bonding modes to new ones, as well as in the interconversion among them by changing the coordination sphere of the metal cluster centers in C_{60}−metal cluster complexes. Our studies have revealed that π-type species can transform into new $\sigma-\pi$ mixed-type ones with μ_3-η^1:η^2:η^1-C_{60} and μ_3-η^1:η^1:η^2-C_{60} ligands by modifying the coordination sphere of metals in the cluster, that is, the C_{60} bonding mode can be remote-controlled by changing the metal cluster environment.[7] The C_{60}−metal σ-complexes are known to be very important starting materials for the selective functionalization of C_{60}. By employing similar approaches, we have observed the elusive μ-η^2:η^2-C_{60} bonding mode in the cluster regime and furthermore have shown that the two bonding modes, μ-η^2:η^2-C_{60} and μ_3-η^2:η^2:η^2-C_{60}, are reversibly interconvertible on an Os_5C cluster framework.[8] More importantly, we have demonstrated an interesting strong electronic communication between C_{60} and metal cluster centers, which can be readily fine-tuned by control of electronic properties of the attached ligands on the metal cluster center.[3a] In our previous work, electrochemical studies of C_{60} derivatives of Re_3,[9] Os_3,[10] and Rh_6[11] clusters have revealed electronic communication between C_{60} and the metal cluster and also strong electronic interaction between C_{60} cages through metal cluster spacers.

Bisfullerene compounds with two electroactive fullerene centers are of special interest because the electronic communication between the two C_{60} centers has practical implications for future applications. A number of bisfullerene compounds with various organic spacers have been prepared in order to effect the electronic communication between the two C_{60} cages. Thus far, however, a weak, through-space electronic communication has been observed only for C_{120},[12] $C_{120}C$,[13] $C_{120}O$,[14] $C_{120}(CH_2)_2$,[15] and $C_{120}Si(C_6H_5)_2$,[16] where the fullerenes are directly bonded to each other or are separated by a single-atom spacer such as carbon, oxygen, and silicon atoms. For organic-based bisfullerenes with longer spacers, on the other hand, no electronic communication has been observed.[17] Insertion of organic spacers between the two C_{60} cages results in the transformation of the hybridization of C_{60} carbon atoms involved in the spacer binding from sp^2 to sp^3, and consequently, the electronic communication is possible only through space via overlapped π-orbitals from the two separate C_{60} cages.

The C_{60}−metal π-interaction in the μ_3-η^2:η^2:η^2-C_{60}−metal clusters little perturbs the C_{60} hybridization, as evidenced by our earlier studies on the self-assembled monolayers,[18] the photovoltaic cell device application,[19] and the X-ray structural characterization of C_{60}−metal cluster π-complexes.[3a] Thus, the electronic properties of bisfullerene complexes with a metal cluster spacer are expected to be drastically different from those of organic-based bisfullerenes. In addition, C_{60}−metal cluster sandwich compounds should serve as direct models for two carbon nanotubes connected by a heterogeneous inorganic junction such as metal nanoparticles. We have recently demonstrated that electron-withdrawing C_{60} cages can be connected by a cluster bridge of octahedral hexarhodium, when the cluster bridge is coordinated with electron-donating phosphine ligands.[11] Cyclic voltammetric and theoretical studies of this bisfullerene−Rh_6 cluster sandwich complex, $Rh_6(CO)_5(dppm)_2(CNCH_2Ph)$-$(\mu_3$-$\eta^2$:$\eta^2$:$\eta^2$-$C_{60})_2$, have shown the presence of unusually strong electronic communication between the two C_{60} centers through the hexarhodium cluster spacer, which is far stronger than that observed for organic-based bisfullerenes (vide infra).[11] Closely following our report of the first hexarhodium bisfullerene sandwich compound, Tang et al. reported the preparation of monometallic bisfullerene sandwich compounds, $[M(\eta^2$-$C_{60})_2$-$(CO)_2(dbcbipy)]$ (M = W and Mo, dbcbipy = 4,4′-di(butylcarboxyl)-2,2′-bipyridine), in which the two trans C_{60} ligands bind to a single metal atom in an η^2 fashion.[20] This compound, however, is electrochemically very unstable similarly as other known η^2-C_{60} metal complexes and reveals very weak inter-fullerene electronic communication comparable to organic-based bisfullerenes.[21]

As an extension of our studies on the chemistry of C_{60}−metal cluster complexes, we have examined the interaction of C_{60} with phosphine-substituted tetrahedral iridium clusters such as $Ir_4(CO)_9(PPh_3)_3$ (**1**) and $Ir_4(CO)_8(PMe_3)_4$ (**4**) in the present

(4) (a) Fagan, P. J.; Calabrese, J. C.; Malone, B. *Science* **1991**, *252*, 1160−1161. (b) Balch, A. L.; Catalano, V. J.; Lee, J. W. *Inorg. Chem.* **1991**, *30*, 3980−3981. (c) Koefod, R. S.; Hudgens, M. F.; Shapley, J. R. *J. Am. Chem. Soc.* **1991**, *113*, 8957−8958. (d) Fagan, P. J.; Calabrese, J. C.; Malone, B. *J. Am. Chem. Soc.* **1991**, *113*, 9408−9409. (e) Douthwaite, R. E.; Green, M. L. H.; Stephens, A. H. H.; Turner, J. F. C. *J. Chem. Soc., Chem. Commun.* **1993**, 1522−1523. (f) Bashilov, V. V.; Petrovskii, P. V.; Sokolov, V. I.; Lindeman, S. V.; Guzey, I. A.; Struchkov, Y. T. *Organometallics* **1993**, *12*, 991−992. (g) Balch, A. L.; Lee, J. W.; Noll, B. C.; Olmstead, M. M. *Inorg. Chem.* **1993**, *32*, 3577−3578. (h) Hsu, H.-F.; Du, Y.; Albrecht-Schmitt, T. E.; Wilson, S. R.; Shapley, J. R. *Organometallics* **1998**, *17*, 1756−1761.

(5) (a) Rasinkangas, M.; Pakkanen, T. T.; Pakkanen, T. A.; Ahlgrén, M.; Rouvinen, J. *J. Am. Chem. Soc.* **1993**, *115*, 4901. (b) Mavunkal, I. J.; Chi, Y.; Peng, S.-M.; Lee, G.-H. *Organometallics* **1995**, *14*, 4454−4456. (c) Chernega, A. N.; Green, M. L. H.; Haggitt, J.; Stephens, A. H. H. *J. Chem. Soc., Dalton Trans.* **1998**, 755−767.

(6) (a) Sawamura, M.; Kuninobu, Y.; Nakamura, E. *J. Am. Chem. Soc.* **2000**, *122*, 12407−12408. (b) Sawamura, M.; Kuninubo, Y.; Toganoh, M.; Matsuo, Y.; Yamanaka, M.; Nakamura, E. *J. Am. Chem. Soc.* **2002**, *124*, 9354−9355. (c) Matsuo, Y.; Nakamura, E. *Organometallics* **2003**, *22*, 2554−2563. (d) Kuninobu, Y.; Matsuo, Y.; Toganoh, M.; Sawamura, M.; Nakamura, E. *Organometallics* **2004**, *23*, 3259−3266. (e) Matsuo, Y.; Iwashita, A.; Nakamura, E. *Organometallics* **2005**, *24*, 89−95.

(7) (a) Song, H.; Lee, K.; Lee, C. H.; Park, J. T.; Chang, H. Y.; Choi, M.-G. *Angew. Chem., Int. Ed.* **2001**, *40*, 1500−1502. (b) Song, H.; Lee, K.; Choi, M.-G.; Park, J. T. *Organometallics* **2002**, *21*, 1756−1758. (c) Song, H.; Lee, C. H.; Lee, K.; Park, J. T. *Organometallics* **2002**, *21*, 2514−2520. (d) Song, H.; Choi, J. I.; Lee, K.; Choi, M.-G.; Park, J. T. *Organometallics* **2002**, *21*, 5221−5228.

(8) (a) Lee, K.; Lee, C. H.; Song, H.; Park, J. T.; Chang, H. Y.; Choi, M.-G. *Angew. Chem., Int. Ed.* **2000**, *39*, 1801−1804. (b) Lee, K.; Choi, Z.-H.; Cho, Y.-J.; Song, H.; Park, J. T. *Organometallics* **2001**, *20*, 5564−5570.

(9) Song, H.; Lee, Y.; Choi, Z.-H.; Lee, K.; Park, J. T.; Kwak, J.; Choi, M.-G. *Organometallics* **2001**, *20*, 3139−3144.

(10) Song, H.; Lee, K.; Park, J. T.; Choi, M.-G. *Organometallics* **1998**, *17*, 4477−4483.

(11) (a) Lee, K.; Song, H.; Kim, B.; Park, J. T.; Park, S.; Choi, M.-G. *J. Am. Chem. Soc.* **2002**, *124*, 2872−2873. (b) Lee, K.; Choi, Y. J.; Cho, Y.-J.; Lee, C. Y.; Song, H.; Lee, C. H.; Lee, Y. S.; Park, J. T. *J. Am. Chem. Soc.* **2004**, *126*, 9837−9844.

(12) Komatsu, K.; Wang, G.-W.; Murata, Y.; Tanaka, T.; Fujiwara, K.; Yamamoto, K.; Saunders, M. *J. Org. Chem.* **1998**, *63*, 9358−9366.

(13) Dragoe, N.; Shimotani, H.; Wang J.; Iwaya, M.; de Bettencourt-Dias, A.; Balch, A. L.; Kitazawa, K. *J. Am. Chem. Soc.* **2001**, *123*, 1294−1301.

(14) Balch, A. L.; Costa, D. A.; Fawcett, W. R.; Winkler, K. *J. Phys. Chem.* **1996**, *100*, 4823−4827.

(15) Dragoe, N.; Shimotani, H.; Hayashi, M.; Saigo, K.; de Bettencourt-Dias, A.; Balch, A. L.; Miyake, Y.; Achiba, Y.; Kitazawa, K. *J. Org. Chem.* **2000**, *65*, 3269−3273.

(16) Fujiwara, K.; Komatsu, K. *Org. Lett.* **2002**, *4*, 1039−1041.

(17) (a) Suzuki, T.; Li, Q.; Khemani, K. C.; Wudl, F. *J. Am. Chem. Soc.* **1992**, *114*, 7300−7301. (b) Murata, Y.; Kato, N.; Fujiwara, K.; Komatsu, K. *J. Org. Chem.* **1999**, *64*, 3483−3488.

(18) Cho, Y.-J.; Song, H.; Lee, K.; Kim, K.; Kwak, J.; Kim, S.; Park, J. T. *Chem. Commun.* **2002**, 2966−2967.

(19) Cho, Y.-J.; Ahn, T. K.; Song, H.; Kim, K. S.; Lee, C. Y.; Seo, W. S.; Lee, K.; Kim, S. K.; Kim, D.; Park, J. T. *J. Am. Chem. Soc.* **2005**, *127*, 2380−2381.

(20) Jin, X.; Xie, X.; Tang, K. *Chem. Commun.* **2002**, 750−751.

(21) Zanello, P.; de Biani, F. F.; Cinquantini, A.; Grigiotti, E. *C. R. Chim.* **2005**, *8*, 1655−1659.

Scheme 1. Structures of **2**, **3**, **5**, and **6**[a]

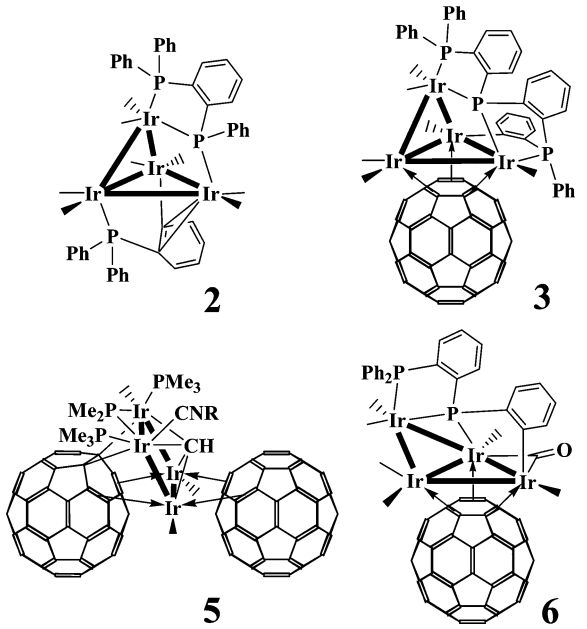

[a] Terminal carbonyl ligands are omitted for clarity.

work. The former reaction affords "butterfly" $Ir_4(CO)_6\{\mu_3\text{-}k^3\text{-}Ph_2P(o\text{-}C_6H_4)PPh(\eta^1\text{-}o\text{-}C_6H_4)\}(\mu_3\text{-}\eta^2\text{:}\eta^2\text{:}\eta^2\text{-}C_{60})$ (**3**) through the intermediate of "butterfly" $Ir_4(CO)_8\{\mu\text{-}\kappa^2\text{-}Ph_2P(o\text{-}C_6H_4)PPh\}\{\mu_3\text{-}PPh(\eta^1\text{:}\eta^2\text{-}o\text{-}C_6H_4)\}$ (**2**) by a series of ortho-phosphorylation and ortho-metalation reactions. The latter reaction produces a bisfullerene−tetrairidium complex, $Ir_4(CO)_3(\mu_4\text{-}CH)(PMe_3)_2(\mu\text{-}PMe_2)(CNCH_2Ph)(\mu\text{-}\eta^2\text{:}\eta^2\text{-}C_{60})(\mu_4\text{-}\eta^1\text{:}\eta^1\text{:}\eta^2\text{:}\eta^2\text{-}C_{60})$ (**5**), after treatment of the insoluble reaction intermediate with $CNCH_2Ph$. Herein we report the full details of syntheses, characterization, and electrochemical properties of **2**, **3**, and **5**, together with electrochemistry of a related known C_{60}−tetrairidium "butterfly" complex $Ir_4(CO)_6(\mu\text{-}CO)\{\mu_3\text{-}\kappa^2\text{-}Ph_2P(o\text{-}C_6H_4)P(\eta^1\text{-}o\text{-}C_6H_4)\}(\mu_3\text{-}\eta^2\text{:}\eta^2\text{:}\eta^2\text{-}C_{60})$ (**6**)[22] (see Scheme 1). To understand the nature of electronic communication between C_{60} and tetrairidium metal cluster center in **3** and **6** and interfullerene communication through a tetrairidium metal spacer in **5**, we have carried out molecular orbital (MO) calculations on a set of face-capping C_{60}−tetrairidium cluster complexes, **3**, **5**, and **6**, by density functional theory (DFT) calculations and charge distribution studies employing the Mulliken (MPA) and Hirshfeld (HPA) population analyses. Preliminary accounts of some of this work have already appeared.[23,24]

Results and Discussion

Synthesis and Characterization of 2, 3, and 5. Heating of tristriphenylphosphine-substituted tetrairidium carbonyl cluster **1** with 2 equiv of C_{60} in refluxing chlorobenzene (CB) for 2 h after usual workup and chromatographic separation gave a novel C_{60}−tetrairidium "butterfly" complex with a triphoshine ligand, **3**, in relatively low yield (36%). Refluxing **1** in CB briefly afforded a "butterfly" tetrairidium complex, **2**, with a diphosphine ligand by ortho-phosphorylation and ortho-metalation reactions in satisfactory yield (64%). More interestingly, treatment of **2** with 2 equiv of C_{60} in refluxing CB for 3 h allowed for the formation of **3** in 41% yield by C_{60}-assisted ortho-phosphorylation reaction, demonstrating that **2** is indeed the reaction intermediate leading to the product **3**. The synthetic details for **2** and **3** are given in Scheme 2. Attempted similar reactions of tristrialkylphosphine-substituted complexes $Ir_4(CO)_8(PR_3)_3$ (R = Me, Et) with C_{60}, however, resulted in only extensive decomposition of the starting materials. On the other hand, reaction of the tetrakistrimethylphosphine-substituted compound, **4**, with excess C_{60} in refluxing 1,2-dichlorobenzene (DCB) for 2 h afforded a new green band on TLC, presumably a carbonyl analogue of **5** which could not be further characterized because of its marginal solubility after solvent removal. Subsequent treatment of the carbonyl analogue with $CNCH_2Ph$ at 70 °C for 2 h produced a green benzyl isocyanide-substituted derivative, **5**, as the major product in low yield (13%), which is soluble enough to be fully characterized. A similar reaction of the tetrakistriethylphosphine-substituted compound $Ir_4(CO)_8(PEt_3)_4$ with C_{60} gave the hydrido monometallic fullerene $Ir(H)(CO)(PEt_3)_2(\eta^2\text{-}C_{60})$ complex,[25] but that of $Ir_4(CO)_8(dppm)_2$ with C_{60} did not afford any isolable product.

Scheme 2. Syntheses of **2** and **3**[a]

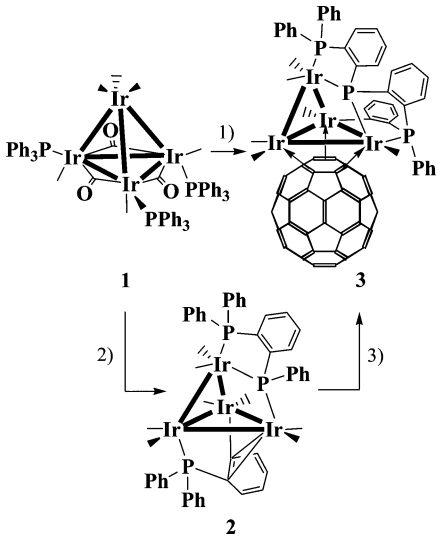

[a] Terminal carbonyl ligands are omitted for clarity.

Compounds **2**, **3**, and **5** were formulated on the basis of elemental analyses and mass spectroscopic data. The FAB^+ mass spectra showed the molecular ion isotope multiplets at *m*/*z* 1624 for **2** and 2210 for **3**. Attempts to obtain mass spectroscopic data for **5**, however, with FAB^+, FAB^-, and MALDI-TOF methods have not been successful. The synthesis and characterization of complex **6** has been discussed in our earlier account.[22]

The ^1H NMR spectrum of **2** shows multiplets in the region of δ 8.44−6.51 due to the 33 aromatic protons of five phenyl and two *o*-phenylene moieties. The $^{31}P\{^1H\}$ NMR spectrum displays two doublets for the diphosphine moiety and a singlet for the monophosphine group. The low-field doublet at δ 24.2 ($^2J_{PP}$ = 22.1 Hz) accounts for the terminal phosphorus atom on a "wing-tip" iridium atom, and the high-field doublet at δ −42.9

(22) Park, B. K.; Miah, M. A.; Kang, H.; Lee, K.; Cho, Y.-J.; Churchill, D. G.; Park, S.; Choi, M.-G.; Park, J. T. *Organometallics* **2005**, *24*, 675−679.
(23) Lee, G.; Cho, Y.-J.; Park, B. K.; Lee, K.; Park, J. T. *J. Am. Chem. Soc.* **2003**, *125*, 13920−13921.
(24) Park, B. K.; Miah, M. A.; Lee, G.; Cho, Y.-J.; Lee, K.; Park, S.; Choi, M,-G.; Park, J. T. *Angew. Chem. Int. Ed.* **2004**, *43*, 1712−1724.
(25) Compound $Ir(H)(CO)(PEt_3)_2(\eta^2\text{-}C_{60})$ was fully characterized by spectroscopic methods, cyclic voltammetry, and a single-crystal X-ray diffraction study.

($^2J_{PP}$ = 22.1 Hz) is assigned to the phosphorus atom that bridges the two "wing-tip" iridium atoms. The singlet at δ 16.4 is obviously assigned to the phosphorus atom on a "hinge" iridium atom. The two resonances at δ 24.2 and 16.4 are consistent with the chemical shift of the terminal phosphorus atom of the triphenylphosphine ligands bonded to an iridium center, usually observed in the region of δ −30 to +70.[26] The ^{13}C NMR spectrum exhibits eight signals at δ 186.8, 185.7, 179.6, 176.4, 166.4, 165.7, 165.5, and 163.7 for eight carbonyl groups and the multiplet resonances around δ 153.2−124.3 assignable to the 42 aromatic carbon atoms.

The ^{1}H NMR spectrum of **3** shows two sets of multiplet resonances around δ 8.07−7.14 and 6.93−6.78 for the 27 aromatic protons of three *o*-phenylene bridges and three phenyl moieties. The ^{31}P{^{1}H} NMR displays two doublets and a doublet of doublet (dd) patterns for the three inequivalent phosphorus atoms of the triphosphine group. The two doublets at δ 31.2 ($^2J_{PP}$ = 12.8 Hz) and at δ 21.5 ($^2J_{PP}$ = 4.0 Hz) are due to the terminal phosphorus atoms on the two "wing-tip" iridium atoms, whereas the dd pattern at δ −16.3 ($^2J_{PP}$ = 12.8 Hz, $^2J_{PP}$ = 4.0 Hz) is assigned to the bridging phosphorus atom. The ^{13}C NMR spectrum reveals six carbonyl resonances at δ 188.4, 187.3, 179.9, 173.3, 172.4, and 161.2 and signals around δ 158.9−143.6 for 54 sp^2 carbon atoms and at δ 79.1, 68.0, 64.1, 62.7, 61.2, and 60.6 for the six π-bonded sp^3 carbon atoms of the C_{60} ligand.

The IR spectrum of complex **5** shows a weak absorption band at 2159 cm^{-1} for the CN stretch of the benzyl isocyanide ligand and a strong CO stretch at 1986 cm^{-1} for the three terminal carbonyl groups. The ^{1}H NMR spectrum contains a characteristic doublet far downfield at δ 15.52 (1H, $^3J_{PH}$ = 13.0 Hz), assigned to the μ_4-CH proton moiety. The phosphorus coupling is assumed to be due to the phosphorus atom of the bridging phosphido group, which is located approximately trans to the methylidyne carbon (vide infra). Similar μ_4-CH groups have been previously reported in various metal clusters such as the square planar complex $Ru_2Pt_2(\mu\text{-H})(\mu_4\text{-CH})(CO)_3(PPr^i_3)_2(\eta^5\text{-}C_5H_5)_2$ (δ_H = 14.87),[27] the edge-sharing bitetrahedral complex $Co_5Mo_2(\mu_4\text{-CH})(\mu_5\text{-C})(CO)_{12}(\eta^5\text{-}C_5H_5)_2$ (δ_H = 12.52),[28] and the square pyramidal complex $Ru_5(\mu\text{-H})(\mu_4\text{-CH})(CO)_{10}(\mu\text{-GePh}_2)_2(\mu_3\text{-GePh})_2$ (δ_H = 11.21).[29] The downfield region shows a multiplet around δ 7.66−7.20 for the five aromatic protons of the benzyl isocyanide ligand. An AB-type doublet around δ 5.18 (2H, $^2J_{HH}$ = 16.5 Hz) accounts for the two diastereotopic benzylic protons of the benzyl isocyanide ligand. The two doublets at δ 2.07 (9H, $^2J_{PH}$ = 9.8 Hz) and 1.86 (9H, $^2J_{PH}$ = 9.1 Hz) are due to the methyl protons of the two inequivalent trimethylphosphine ligands. The two sets of doublet at δ 3.55 (3H, $^2J_{PH}$ = 7.0 Hz) and 3.04 (3H, $^2J_{PH}$ = 4.6 Hz) have been assigned to the two diastereotopic methyl groups on the bridging phosphido moiety. The ^{31}P{^{1}H} NMR spectrum exhibits three singlets at δ 164.3, −44.9, and −47.9. The lowest-field signal is assigned to the bridging phosphorus atom, commonly observed in the downfield region of δ 130−300,[26] whereas the two high-field resonances are due to the terminal phosphorus atoms of the trimethylphosphine ligands which usually appear in the δ −30 to −70 region.[26]

Scheme 3 [a]

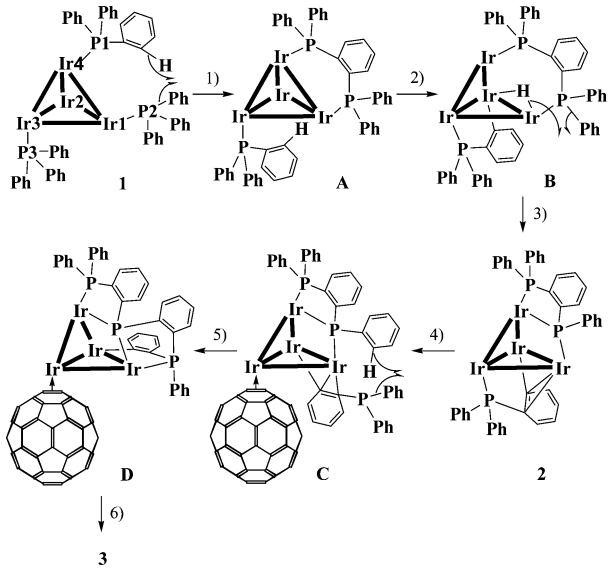

[a] (1) −C_6H_6; 2) ortho-metalation of a phenyl group on the P3; (3) −C_6H_6, −CO; (4) + C_{60}; (5) −C_6H_6; (6) −2CO. Carbonyl ligands are omitted for clarity.

A plausible reaction mechanism for the conversion of **1** → **2** → **3** is proposed in Scheme 3. The first step is an ortho-phosphorylation in **1** to form the bidentate diphosphine intermediate **A**. Ortho-metalation of a phenyl group on the P3 atom in **A** results in the Ir1−Ir4 bond rupture to form the hydrido butterfly intermediate **B** (62 valence electrons (VEs)); a similar conversion was previously reported for tetrairidium clusters.[22] Binuclear reductive elimination of C_6H_6 and loss of a carbonyl ligand in **B** induces coordination of the P2 atom to the Ir4 center and π-coordination of the ortho-metalated phenyl ring to the Ir1 atom to form an η^1:η^2-*o*-C_6H_4 moiety in **2**. The next step is cleavage of the Ir3−P3 bond and subsequent coordination of η^2-C_{60} to produce the intermediate **C**. Another ortho-phosphorylation reaction in **C** takes place to form a triphosphine moiety, and the π-interaction in the η^1:η^2-*o*-C_6H_4 ligand is replaced by coordination of the P3 atom to the Ir1 center to give the intermediate **D**. The final product **3** is produced by the loss of two carbonyl ligands and formation of face-capping of the C_{60} ligand in μ_3-η^2:η^2:η^2 fashion. In this transformation, three PPh_3 ligands are converted to the diphosphine μ-PPh_2(*o*-C_6H_4)PPh in **2** and in turn to the triphosphine μ_3-PPh_2(*o*-C_6H_4)P(*o*-C_6H_4)-PPh(η^1-*o*-C_6H_4) in **3** on the tetrairidium cluster framework by successive ortho-phosphorylation and ortho-metalation processes.

Synthesis of phosphine ligands with P−(C)$_n$−P and P−(C)$_n$−P−(C)$_n$−P donor sequences is of special interest because of their ability to bridge metal−metal bonds and thus to stabilize organometallic or metal cluster complexes. Such phosphine ligands have usually been prepared by tedious multistep organic synthesis.[30] Instances in which phosphines couple to form a diphosphine in transition metal complexes are extremely rare, with only two other examples known, one for a Pd monomer[31]

(26) (a) Pregoein, P. S.; Kunz, R. W. *^{31}P and ^{13}C NMR Studies of Transition Metal Phosphine Complexes*; Springer-Verlag: New York, 1979. (b) Garrou, P. E. *Chem. Rev.* **1981**, *81*, 229−266. (c) Goh, L. Y.; Weng, Z.; Leong, W. K.; Vittal, J. J.; Haiduc, I. *Organometallics* **2002**, *21*, 5287−5291. (d) Ziglio, C. M.; Vargas, M. D.; Braga, D.; Grepioni, F.; Nixon, J. F. *J. Organomet. Chem.* **2002**, *656*, 188−198.
(27) (a) Davies, D. L.; Jeffery, J. C.; Miguel, D.; Sherwood, P.; Store, F. G. A. *J. Chem. Soc., Chem. Commun.* **1987**, 454−456. (b) Davies, D. L.; Jeffery, J. C.; Miguel, D.; Sherwood, P.; Stone, F. G. A. *J. Organomet. Chem.* **1990**, *383*, 463−480.
(28) Adams, H.; Guio, L. V. Y.; Morris, M. J.; Spey, S. E. *J. Chem. Soc., Dalton Trans.* **2002**, 2907−2915.
(29) Adams, R. D.; Captain, B.; Fu, W. *Inorg. Chem.* **2003**, *42*, 1328−1333.

Table 1. Selected Interatomic Distances (Å) and Bond Angles (deg) for **2**

Bond Distances			
Ir(1)−Ir(2)	2.6953(6)	Ir(1)−Ir(3)	2.7170(7)
Ir(2)−Ir(3)	2.6689(6)	Ir(2)−Ir(4)	2.7409(6)
Ir(3)−Ir(4)	2.8054(6)	Ir(1)−P(2)	2.297(3)
Ir(3)−P(3)	2.286(3)	Ir(4)−P(2)	2.309(3)
Ir(4)−P(1)	2.295(3)	Ir(1)−C(701)	2.55(1)
Ir(1)−C(706)	2.41(1)	Ir(2)−C(706)	2.08(1)
P(1)−C(301)	1.81(1)	P(2)−C(306)	1.86(1)
P(3)−C(701)	1.82(1)		
Bond Angles			
Ir(2)−Ir(1)−Ir(3)	59.09(2)	Ir(3)−Ir(2)−Ir(4)	62.46(2)
Ir(3)−Ir(2)−Ir(1)	60.86(2)	Ir(4)−Ir(2)−Ir(1)	88.20(2)
Ir(2)−Ir(3)−Ir(4)	60.03(2)	Ir(2)−Ir(3)−Ir(1)	60.05(2)
Ir(4)−Ir(3)−Ir(1)	86.46(2)	Ir(2)−Ir(4)−Ir(3)	57.51(2)
P(2)−Ir(1)−Ir(2)	76.79(8)	P(2)−Ir(1)−Ir(3)	74.04(7)
P(2)−Ir(4)−P(1)	87.3(1)	P(2)−Ir(4)−Ir(3)	72.12(7)
P(1)−Ir(4)−Ir(3)	96.58(8)	Ir(1)−P(2)−Ir(4)	110.5(1)
P(2)−Ir(4)−Ir(2)	75.66(8)	P(1)−Ir(4)−Ir(2)	152.18(8)
P(3)−Ir(3)−Ir(2)	83.51(8)	P(3)−Ir(3)−Ir(1)	76.62(8)
P(3)−Ir(3)−Ir(4)	143.44(8)	C(306)−P(2)−Ir(4)	106.4(3)
C(301)−C(306)−P(2)	117.8(8)	C(301)−P(1)−Ir(4)	108.3(4)
C(306)−C(301)−P(1)	118.9(9)	P(2)−Ir(1)−C(706)	123.1(3)
P(2)−Ir(1)−C(701)	145.7(3)	Ir(3)−Ir(2)−C(706)	93.6(3)
Ir(3)−P(3)−C(701)	108.3(4)	P(3)−C(701)−C(706)	115.5(8)
C(701)−C(706)−Ir(2)	121.0(8)		

Table 2. Selected Interatomic Distances (Å) and Bond Angles (deg) for **3**

Bond Distances			
Ir(1)−Ir(2)	2.7598(8)	Ir(1)−Ir(3)	2.7827(8)
Ir(2)−Ir(3)	2.8059(7)	Ir(2)−Ir(4)	2.7401(9)
Ir(3)−Ir(4)	2.8094(7)	Ir(4)−P(1)	2.318(2)
Ir(4)−P(2)	2.300(2)	Ir(1)−P(3)	2.282(2)
Ir(1)−P(2)	2.281(2)	Ir(2)−C(502)	2.089(8)
P(1)−C(301)	1.826(9)	P(2)−C(306)	1.841(8)
P(2)−C(401)	1.831(9)	P(3)−C(406)	1.807(9)
P(3)−C(501)	1.812(9)	Ir(1)−C(1)	2.256(8)
Ir(1)−C(2)	2.222(8)	Ir(2)−C(3)	2.241(8)
Ir(2)−C(4)	2.150(8)	Ir(3)−C(5)	2.303(8)
Ir(3)−C(6)	2.161(8)	C(1)−C(2)	1.44(1)
C(2)−C(3)	1.49(1)	C(3)−C(4)	1.42(1)
C(4)−C(5)	1.48(1)	C(5)−C(6)	1.43(1)
C(6)−C(1)	1.51(1)		
Bond Angles			
Ir(2)−Ir(1)−Ir(3)	60.83(1)	Ir(3)−Ir(2)−Ir(4)	60.86(1)
Ir(3)−Ir(2)−Ir(1)	59.99(2)	Ir(4)−Ir(2)−Ir(1)	85.02(1)
Ir(2)−Ir(3)−Ir(4)	58.42(2)	Ir(2)−Ir(3)−Ir(1)	59.18(2)
Ir(4)−Ir(3)−Ir(1)	83.30(2)	Ir(2)−Ir(4)−Ir(3)	60.73(2)
P(2)−Ir(1)−Ir(2)	77.56 (6)	P(2)−Ir(1)−Ir(3)	76.57(7)
P(2)−Ir(4)−P(1)	85.87(8)	P(2)−Ir(4)−Ir(3)	75.72(6)
P(1)−Ir(4)−Ir(3)	101.28(6)	Ir(1)−P(2)−Ir(4)	108.45(9)
P(2)−Ir(4)−Ir(2)	77.67 (6)	P(1)−Ir(4)−Ir(2)	158.00(8)
P(3)−Ir(1)−Ir(2)	85.87(6)	P(3)−Ir(1)−Ir(3)	144.33(6)
P(2)−Ir(1)−P(3)	84.53(8)	Ir(4)−P(1)−C(301)	108.2(3)
Ir(4)−P(2)−C(306)	107.6(3)	P(1)−C(301)−C(306)	116.8(6)
P(2)−C(306)−C(301)	119.2(7)	Ir(1)−P(2)−C(401)	108.1(3)
Ir(1)−P(3)−C(406)	108.8(3)	P(2)−C(401)−C(406)	118.4(7)
P(3)−C(406)−C(401)	115.9(7)	Ir(1)−P(3)−C(501)	114.2(3)
Ir(1)−Ir(2)−C(502)	94.7(2)	P(3)−C(501)−C(502)	119.9(6)
Ir(2)−C(502)−C(501)	122.6(6)		

and one for an Ir_4 cluster.[22] Further coupling leading to the formation of triphosphine as assisted by C_{60} shown in the present work is unprecedented and remarkable (Scheme 3).

To address the origin of the face-capping μ_4-CH unit in **5**, the reaction of deuterated $Ir_4(CO)_8(P(CD_3)_3)_4$ with C_{60}, followed by treatment with benzyl isocyanide, was carried out. The μ_4-CH signal at δ 15.52 is absent in the ^{1}H NMR spectrum of the formed deuterium-labeled phosphine analogue of **5** (**5d**), implying that a methyl group in a PMe_3 ligand is the source of the resultant methylidyne moiety by P−C and C−H bond activation. Since three phosphorus atoms remain in **5**, reaction of stoichiometrically precise $Ir_4(CO)_9(PMe_3)_3$ with C_{60} was attempted, but resulted in severe decomposition of the starting material. Additional PMe_3 ligand in the starting material, **4**, apparently plays a crucial role in the formation of **5**. Efforts to prepare a μ_4-CCH_3 complex have not been successful by employing $Ir_4(CO)_8(PEt_3)_4$, but the hydrido monoiridium $Ir(H)(CO)(PEt_3)_2(\eta^2\text{-}C_{60})$ compound was produced by extensive fragmentation of the tetrairidium framework, which will be reported elsewhere.[25]

X-ray Crystal Structures of 2, 3, and 5. Selected interatomic distances and angles of **2**, **3**, and **5** are listed in Tables 1−3, respectively.

The molecular structures of **2** and **3** are shown in Figures 1 and 2, respectively. Both complexes exhibit a "butterfly" geometry of four iridium atoms as expected for 62 VE metal clusters. The two "wings" are nearly perpendicular to each other ($\angle$Ir4−Ir2−Ir1 = 88.20(2)° for **2** and 85.02(1)° for **3**), as was observed in previously reported "wing-tip" bridged tetrairidium "butterfly" complexes.[32a] The bond length of the Ir3−Ir4 is relatively longer (2.8054(6) Å for **2** and 2.8094(7) Å for **3**) than the other Ir−Ir distances in both **2** and **3**. However, the average Ir−Ir distances of 2.7255(6) and 2.7796(8) Å of **2** and **3** are comparable to those observed in other known "butterfly" tetrairidium clusters.[32] Each iridium atom of **2** has two terminal carbonyl groups. The P1 atom bearing two phenyl groups in **2** is coordinated to the Ir4 center, and the two "wing-tip" Ir atoms are almost symmetrically bridged by the P2 atom (Ir1−P2 = 2.297(3) Å and Ir4−P2 = 2.309(3) Å) with $\angle$Ir1−P2−Ir4 = 110.5(1)°. An *o*-phenylene group bridges the P1 and P2 atoms in the bidentate diphosphine moiety $Ph_2P(o\text{-}C_6H_4)PPh$, which in turn forms a five-membered metalacyclic P1−C301−C306−P2−Ir4 moiety on the cluster. Another interesting feature of **2** is the presence of μ_3-$PPh_2(\eta^1{:}\eta^2\text{-}o\text{-}C_6H_4)$ ligand (a five-electron donor), which is coordinated through P3 to the Ir3 atom, by an Ir−C(phenylene) σ-bond to the Ir2 center, and by an η^2 interaction of the o-C_6H_4 ring to the Ir1 atom to form another metalacycle Ir3−P3−C701−C706−Ir2. A similar five-electron-donor bonding mode was previously observed in $(\mu\text{-H})Os_3(CO)_8\{\mu_3\text{-PPhMe}(\eta^1{:}\eta^2\text{-}C_6H_4)\}$[33] and $(\mu\text{-H})Ru_3(CO)_8\{\mu_3\text{-PPh}(\eta^1{:}\eta^2\text{-}C_6H_4)(\eta\text{-}C_5H_4)Fe(\eta\text{-}C_5H_4PPh_2)\}$.[34] In compound **3**, one terminal carbonyl group is bonded to each of Ir1 and Ir2 atoms, whereas each of the Ir3 and Ir4 centers is ligated by two terminal carbonyl groups. The P1 atom bearing two phenyl groups is

(30) (a) Bianchini, C.; Frediani, P.; Sernau, V. *Organometallics* **1995**, *14*, 5458−5459. (b) Hietkamp, S.; Sommer, H.; Stelzer, O. *Inorg. Synth.* **1989**, *25*, 120−122. (c) Hartley, J. G.; Venanzi, L. M.; Goodall, D. C. *J. Chem. Soc.* **1963**, 3930−3936.

(31) Estevan, F.; García-Bernabé, A.; Lahuerta, P.; Sanaú, M.; Ubeda, M. A.; Galán-Mascaros, J. R. *J. Organomet. Chem.* **2000**, *596*, 248−251.

(32) (a) Stuntz, G. F.; Shapley, J. R.; Pierpont, C. G. *Inorg. Chem.* **1978**, *17*, 2596−2603. (b) Vargas, M. D.; Pereira, R. M. S.; Braga, D.; Grepioni, F. *J. Chem. Soc., Chem. Commun.* **1993**, 1008−1010. (c) Benvenutti, M. H. A.; Vargas, M. D.; Braga, D.; Grepioni, F.; Mann, B. E.; Naylor, S. *Organometallics* **1993**, *12*, 2947−2954. (d) Benvenutti, M. H. A.; Vargas, M. D.; Braga, D.; Grepioni, F.; Parisini, E.; Mann, B. E. *Organometallics* **1993**, *12*, 2955−2961 and references therein; (e) Pereira, R. M. S.; Fijiwara, F. Y.; Vargas, M. D.; Braga, D.; Grepioni, F. *Organometallics* **1997**, *16*, 4833−4838. (f) Araujo, M. H.; Hitchcock, P. B.; Nixon, J. F.; Vargas, M. D. *J. Braz. Chem. Soc.* **1998**, *9*, 563−570.

(33) Deeming, A. J.; Kabir, S. E.; Powell, N. I.; Bates, P. A.; Hursthouse, M. B. *J. Chem. Soc., Dalton Trans.* **1987**, 1529−1534.

(34) Bruce, M. I.; Humphrey, P. A.; Shawkataly, O. B.; Snow, M. R.; Tiekink, E. R. T.; Cullen, W. R. *Organometallics* **1990**, *9*, 2910−2919.

Table 3. Selected Interatomic Distances (Å) and Bond Angles (deg) for **5**

	Bond Distances		
Ir(1)−Ir(2)	3.0388(7)	Ir(1)−Ir(4)	2.8574(7)
Ir(2)−Ir(3)	2.9116(7)	Ir(3)−Ir(4)	2.7819(7)
Ir(3)−P(3)	2.313(4)	Ir(3)−P(1)	2.372(4)
Ir(4)−P(3)	2.284(3)	Ir(4)−P(2)	2.318(4)
Ir(1)−C(1)	2.20(1)	Ir(1)−C(3′)	2.11(1)
Ir(1)−C(2)	2.16(1)	Ir(1)−C(4′)	2.20(1)
Ir(2)−C(3)	2.17(1)	Ir(2)−C(1′)	2.19(1)
Ir(2)−C(4)	2.19(1)	Ir(2)−C(2′)	2.14(1)
Ir(3)−C(5)	2.17(1)	Ir(4)−C(6)	2.19(1)
C(1′)−C(2′)	1.46(2)	C(1′)−C(6′)	1.52(2)
C(2′)−C(3′)	1.50(2)	C(3′)−C(4′)	1.48(2)
C(4′)−C(5′)	1.50(2)	C(5′)−C(6′)	1.36(2)
C(1)−C(2)	1.44(2)	C(2)−C(3)	1.49(2)
C(3)−C(4)	1.49(2)	C(4)−C(5)	1.50(2)
C(5)−C(6)	1.55(2)	C(1)−C(6)	1.54(2)
C(100)−H(100)	1.10(2)		
	Bond Angles		
Ir(3)−Ir(2)−Ir(1)	87.41(2)	Ir(4)−Ir(1)−Ir(2)	87.47(2)
Ir(3)−Ir(2)−Ir(1)	87.41(2)	Ir(4)−Ir(3)−Ir(2)	91.47(2)
P(3)−Ir(3)−P(1)	100.2(2)	P(1)−Ir(3)−Ir(4)	112.3(1)
P(3)−Ir(3)−Ir(4)	52.28(9)	P(3)−Ir(4)−P(2)	103.8(1)
P(3)−Ir(3)−Ir(2)	143.67(9)	P(1)−Ir(3)−Ir(2)	95.91(9)
P(3)−Ir(4)−Ir(3)	53.3(1)	P(2)−Ir(4)−Ir(3)	154.35(9)
Ir(4)−P(3)−Ir(3)	74.5(1)	P(3)−Ir(4)−Ir(1)	146.8(1)
P(2)−Ir(4)−Ir(1)	107.75(9)	Ir(3)−Ir(4)−Ir(1)	93.64(2)

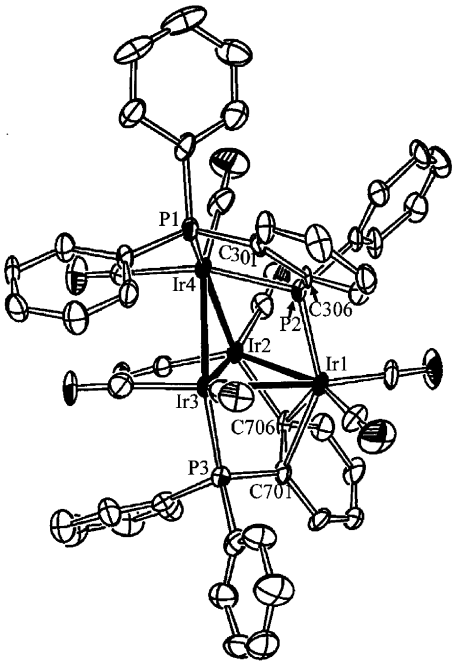

Figure 1. Molecular geometry and atomic-labeling scheme for **2**.

coordinated to the Ir4 atom, and the two "wing-tip" Ir1 and Ir4 atoms are spanned slightly asymmetric by P2 (Ir4−P2 = 2.300(2) Å and Ir1−P2 = 2.281(2) Å) with an angle of 108.45(9)° (∠Ir4−P2−Ir1). The phenyl group on the P2 atom has been ortho-phosphorylated by the P3 atom, and a phenyl group on the P3 center underwent ortho-metalation to form two five-membered Ir1−P2−C401−C406−P3 and Ir1−Ir2−C502−C501−P3 metalacycles, respectively. Overall, the three phosphine ligands in **1** are converted to a triphosphine ligand PPh_2(*o*-C_6H_4)P(*o*-C_6H_4)PPh(η^1-*o*-C_6H_4) in **3**. The C_{60} ligand in **3** is coordinated to the lower "wing" of the "butterfly" composed of the Ir1−Ir2−Ir3 triangle in a typical μ_3-η^2:η^2:η^2-C_{60} arene-type fashion, which has recently been reviewed.[3a] The C−C

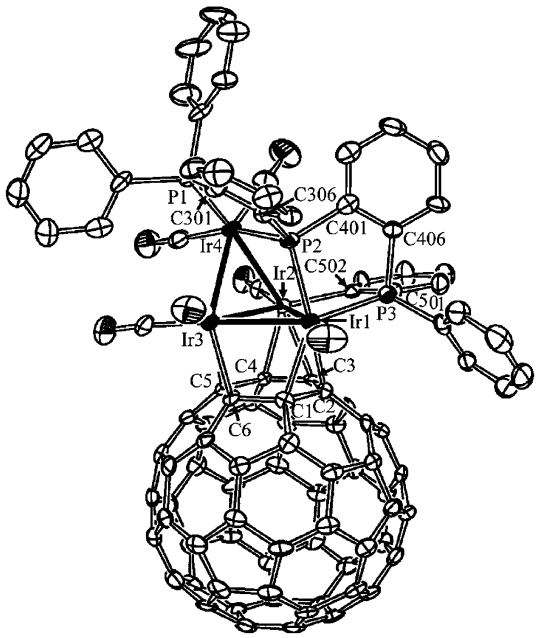

Figure 2. Molecular geometry and atomic-labeling scheme for **3**.

bonds in the μ_3-η^2:η^2:η^2-C_{60} ligand alternate in length, with an average long distance of 1.49(1) Å and average short distance of 1.43(1) Å. The formal electron counts for Ir1, Ir2, Ir3, and Ir4 of **2** and **3** are 18, 17, 18, and 19, respectively. The formal electron deficiency at the Ir2 center appears to be compensated for by a strong σ-interaction (2.08(1) Å) between Ir2 and C706 in **2** and similarly between Ir2 and C502 (2.089(8) Å) in **3**.

The molecular structure of **5** is shown in Figure 3. Extensive structural changes have occurred for the tetrairidium metal framework and ligand coordination environments from the starting complex. The tetrairidium metal framework in **5** now has a square-planar geometry, whereas the starting material $Ir_4(CO)_8(PMe_3)_4$ adopts a tetrahedral core. The overall VE count is 64 VEs for **5**, as expected for a four-metal cluster compound with a square-planar geometry. The tetrairidium framework is face-capped, surprisingly, by a methylidyne unit which formally acts as a three-electron donor. The C−H bond vector is almost perpendicular to the square-planar tetrairidium plane, and the bond length is 1.10(2) Å, which compares with those of $Ru_2Pt_2(\mu\text{-H})(\mu_4\text{-CH})(CO)_3(PPr^i_3)_2(\eta^5\text{-}C_5H_5)_2$ (1.0(1) Å)[27] and $Ru_5(\mu\text{-H})(\mu_4\text{-CH})(CO)_{10}(\mu\text{-GePh}_2)_2(\mu_3\text{-GePh})_2$ (0.89(2) Å).[29] The Ir3 and Ir4 metal atoms, each coordinated with a terminal PMe_3 ligand, are bridged by a PMe_2 moiety. A benzyl isocyanide ligand is coordinated to the Ir4 atom, and one terminal carbonyl ligand is bonded to each of the Ir1, Ir2, and Ir3 atoms. Interesting structural features are observed for the C_{60}−metal interactions; two adjacent metals, Ir1 and Ir2, bridge the two C_{60} units via a μ-η^2:η^2-C_{60} bonding mode. The inner carbon atoms, C(2, 3) and C(2′, 3′), of the butadiene-like moieties of the two C_{60} units exhibit stronger interactions with metal atoms than the outer carbon atoms, C(1, 4) and C(1′, 4′), as was previously observed for $Os_5C(CO)_{12}(PPh_3)(\mu\text{-}\eta^2\text{:}\eta^2\text{-}C_{60})$:[8] Ir1−C2 = 2.16(1) Å; Ir2−C3 = 2.17(1) Å; Ir2−C2′ = 2.14(1) Å; Ir1−C3′ = 2.11(1) Å; Ir1−C1 = 2.20(1) Å; Ir2−C4 = 2.19(1) Å; Ir2−C1′ = 2.19(1) Å; Ir1−C4′ = 2.20(1) Å. More importantly, the other two metal atoms, Ir3 and Ir4, bind to two carbon atoms (C5 and C6) of one C_{60} unit in a σ-fashion, which is the first example of a novel $\sigma-\pi$ mixed-type μ_4-η^1:η^1:η^2:η^2-C_{60} bonding mode. The σ-in-

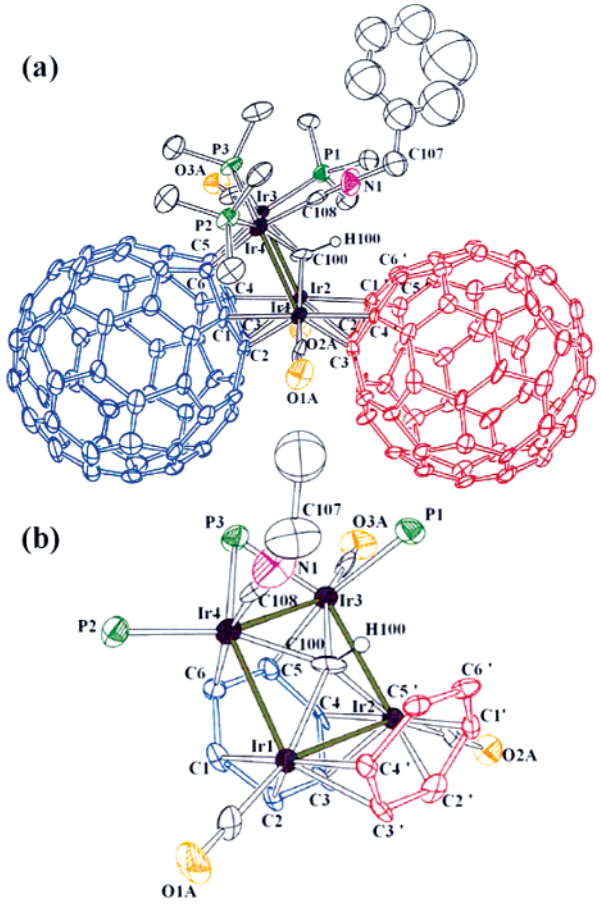

Figure 3. (a) Molecular geometry and atomic-label scheme for **5**. (b) Expanded view of ligated C_6 rings of the two C_{60} ligands.

teractions (Ir3−C5 = 2.17(1) Å and Ir4−C6 = 2.19(1) Å) are comparable to the σ-type interactions (2.11(1)−2.20(1) Å) unlike other known $\sigma-\pi$ mixed complexes such as $Os_3(CO)_8(L)(\mu_3\text{-}CNR)(\mu_3\text{-}\eta^1\text{:}\eta^2\text{:}\eta^1\text{-}C_{60})$ (L = CO, CNR; R = CH_2Ph) and $Os_3(CO)_7(CNR)(\mu_3\text{-}CNR)(L)(\mu_3\text{-}\eta^1\text{:}\eta^2\text{:}\eta^1\text{-}C_{60})$ (L = $(\mu\text{-H})_2$, CNR, PMe_3; R = CH_2Ph), in which shorter bond distances are commonly observed for σ-bonds (2.19(2)−2.25(2) Å) compared to π-bonds (2.31(2)−2.50(2) Å).[7] The C_6 ring in the $\mu\text{-}\eta^2\text{:}\eta^2\text{-}C_{60}$ ligand shows alternation in C−C bond distances (av 1.43(2) and 1.51(2) Å, respectively). However, the other C_6 ring in the $\mu_4\text{-}\eta^1\text{:}\eta^1\text{:}\eta^2\text{:}\eta^2\text{-}C_{60}$ ligand exhibits 1,3-cyclohexadiene-like nature; the bond lengths, C1−C2 (1.44(2) Å) and C3−C4 (1.49(2) Å), are shorter than the other four C−C bonds (av 1.52(2) Å). The sums of three angles around sp^3-hybridized C5 (334°) and C6 (333°) are considerably smaller than those of the other four carbon atoms (av 347°) with sp^2 hybridization. Similar protrusion of sp^3-hybridized carbons from the smooth curvature of the C_{60} ligand has been previously observed for related $\sigma-\pi$ mixed-type C_{60}-cluster complexes.[7] To our knowledge, the only previously known square-planar tetrairidium compound is $Ir_4(CO)_8\{C_2(CO_2Me)\}_4$[35] with 64 VEs which contains four acetylene ligands: two functions as four-electron donors and two as two electron donors.

All the bond distances and angles for **2**, **3**, and **5**, including those for the carbonyl and C_{60} ligands, are within the expected ranges.

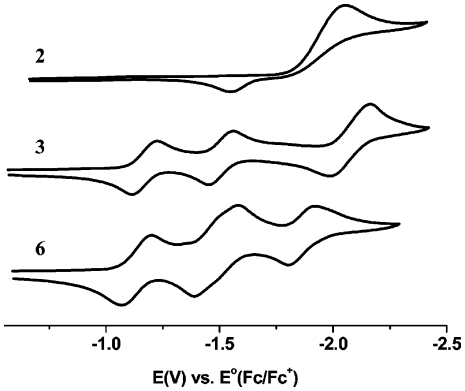

Figure 4. CVs of **2**, **3**, and **6** in chlorobenzene (scan rate = 50 mV/s).

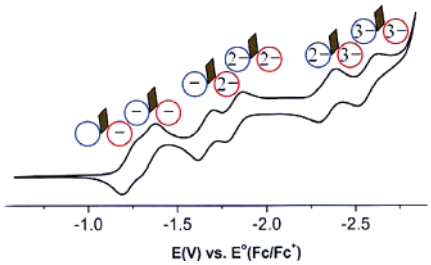

Figure 5. CV of **5** in chlorobenzene (scan rate = 10 mV/s).

Electrochemical Studies of 2, 3, 5, and 6. The electrochemical properties of compounds **2**, **3**, **5**, and **6** in CB have been examined by cyclic voltammetry with tetrabutylammonium perchlorate as the supporting electrolyte. Cyclic voltammograms (CVs) of **2**, **3**, and **6** are shown in Figure 4, and that of **5** is shown in Figure 5. Half-wave potentials ($E_{1/2}$) of all the new compounds, together with free C_{60},[36] $Os_3(CO)_8(PMe_3)(\mu_3\text{-}\eta^2\text{:}\eta^2\text{:}\eta^2\text{-}C_{60})$ (**7**),[10] $Os_3(CO)_8(CN(CH_2)_3Si(OEt)_3)(\mu_3\text{-}\eta^2\text{:}\eta^2\text{:}\eta^2\text{-}C_{60})$ (**8**),[18] and $Rh_6(CO)_5(dppm)_2(CNCH_2Ph)(\mu_3\text{-}\eta^2\text{:}\eta^2\text{:}\eta^2\text{-}C_{60})_2$ (**9**),[11] are provided in Table 4.

The CV of tetrairidiumcomplex **2** exhibits an irreversible two-electron reduction at −2.04 V and reoxidation at −1.53 V of the material formed during the reduction, which has been evidenced by the observation that no waves were observed by scanning between −0.4 and −1.7 V. Similar irreversible behaviors have been commonly observed for metal carbonyl cluster complexes, where loss of a carbonyl and structural changes are generally accompanied by a two-electron reduction.[37] The CV of triphosphine-coordinated C_{60}−tetrairidium complex **3** reveals four reversible redox couples that each correspond to a one-electron processes with the third and fourth waves overlapped within the CB solvent potential window. The general features of the CV of **3** are similar to those of the previously reported complexes **7**[10] and **8**,[18] as listed in Table 4. All the four-half-wave potentials of **3**, however, appear at much

(35) Heveldt, P. F.; Johnson, B. F. G.; Lewis, J.; Raithby, P. R.; Sheldrick, G. M. *J. Chem. Soc., Chem. Commun.* **1978**, 340−341.

(36) (a) Xie, Q.; Perez-Cordero, E.; Echegoyen, L. *J. Am. Chem. Soc.* **1992**, *114*, 3978−3980. (b) Ohsawa, Y.; Saji, T. *J. Chem. Soc., Chem. Commun.* **1992**, 781−782. (c) Zhou, F.; Jehoulet, C.; Bard, A. J. *J. Am. Chem.* Soc. **1992**, *114*, 11004−11006.

(37) (a) Geiger, W. E.; Connelly, N. G. *Adv. Organomet. Chem.* **1985**, *24*, 87−130. (b) Johnson, B. F. G.; Lewis, J.; Nelson, W. J. H.; Nicholls, J. N.; Puga, J.; Raithby, P. R.; Rosales, M. J.; Schröder, M.; Vargas, M. D. *J. Chem. Soc., Dalton Trans.* **1983**, 2447−2457. (c) Clark, R. J. H.; Dyson, P. J.; Humphrey, D. G.; Johnson, B. F. G. *Polyhedron* **1998**, *17*, 2985−2991. (d) Shephard, D. S.; Johnson, B. F. G.; Harrison, A.; Parsons, S.; Smidt, S. P.; Yellowlees, L. J.; Reed, D. *J. Organomet. Chem.* **1998**, *563*, 113−136.

Table 4. Half-Wave Potentials ($E_{1/2}$ vs E°_{Fc/Fc^+}) of C_{60}, **2**, **3**, **5**, **6**, **7**, **8**, and **9**

compound	$E_{1/2}^{0/-1}$	$E_{1/2}^{-1/-2}$	$E_{1/2}^{-2/-3}$	$E_{1/2}^{-3/-4}$	$E_{1/2}^{-4/-5}$	$E_{1/2}^{-5/-6}$	solvent	ref
C_{60}	−1.06	−1.43	−1.91	−2.38			CB	9
2		−2.04[a]					CB	*b*
3	−1.18	−1.53	−2.11	−2.11			CB	*b*
7	−1.06	−1.42	−1.93	−1.95			DCB	10
8	−1.01	−1.37	−1.81	−1.81			DM	18
6	−1.13	−1.46	−1.54	−1.88			CB	*b*
5	−1.25	−1.32	−1.66	−1.82	−2.35	−2.58	CB	23
9	−1.19	−1.38	−1.62	−1.86	−2.12	−2.41	CB	11

[a] Two-electron process and peak potential of irreversible process. [b] This work.

more negative potentials, at least by ca. 120 mV, compared to those of **7** and **8**, since compound **3** contains a strongly electron-donating triphosphine ligand. The first through third reduction potentials of **3** (−1.18, −1.53, and −2.11 V), show large cathodic shifts compared to those of free C_{60} (−1.06, −1.43, and −1.91 V) due to donor effects of both iridium metals and the triphosphine ligand, which indicates that compound **3** undergoes three successive C_{60}-localized reductions to produce $\mathbf{3}^{-}$, $\mathbf{3}^{2-}$, and $\mathbf{3}^{3-}$ (vide infra). The third and fourth reductions of **3**, however, take place at the same potential (−2.11 V), which is even more positive than the fourth redox wave of free C_{60} at −2.38 V. The overlap of the third and fourth waves in **3**, **7**, and **8** support the general conclusion that the electron density of C_{60} in the species $\mathbf{3}^{3-}$, $\mathbf{7}^{3-}$, and $\mathbf{8}^{3-}$ is significantly delocalized to the metal cluster center.[3a,38] Accordingly, the fourth electron can add to the C_{60} moiety of $\mathbf{3}^{3-}$, $\mathbf{7}^{3-}$, and $\mathbf{8}^{3-}$ more easily compared to free C_{60}^{3-}, which results in a large positive shift of the fourth reduction potential of **3** (270 mV), **7** (430 mV), and **8** (570 mV) relative to free C_{60}, as shown in Table 4. The CV of diphosphine-coordinated C_{60}−tetrairidium complex **6** reveals four reversible redox waves, each corresponding to a one-electron process. The second and third redox waves are very close but could be resolved into two one-electron redox couples at half-wave potentials of −1.46 and −1.54 V by simulation using PeakFit 4.11 software,[39] as listed in Table 4. The third redox wave at −1.54 V appears at a much more positive potential than that of free C_{60} at −1.91 V, which also implies that the electron density in dianionic species $\mathbf{6}^{2-}$ is significantly delocalized from C_{60} to the tetrairidium cluster center, resulting in an unusually large anodic shift (370 mV) of the third redox wave compared to that of the free C_{60}. The following redox wave at −1.88V is due to one-electron C_{60}-localized reduction to form $\mathbf{6}^{4-}$ (vide infra). The electron delocalization from C_{60} to the tetrairidium cluster is also reflected in the fourth reduction (−1.88 V) of **6** with an anodic shift (500 mV) compared to free C_{60} reduction (−2.38 V).

The first two reductions for **3** and all four reductions of **6** occur at much more positive potentials compared to the "butterfly" tetrairidium cluster reduction (E_{red} = −2.04 V) of **2**, and thus could be confidently assigned to the C_{60}-localized successive reductions. The overlapped third and fourth one-electron reductions of **3** were assigned to redox processes also localized on the C_{60} ligand, based on MO calculation results (vide infra). All the corresponding half-wave-potentials of **6** are more positive than those of **3**, revealing a clearly less electron-donating nature of the diphosphine ligand in **6** in comparison with the triphosphine ligand in **3**. The half-wave potential data in Table 4 indicate that corresponding reduction potentials of each compound generally decrease as **8** > **7** > **6** > **3**, implying that electron-donating power of ligands decreases as triphosphine > diphosphine > PMe_3 > $CN(CH_2)_3Si(OEt)_3$, as commonly expected for a ligand donor effect. Furthermore, these data suggest that half-wave potentials of C_{60}−metal cluster complexes can be readily fine-tuned by changing the coordinated ligands. This class of complexes, therefore, would certainly invoke an increased interest in future electronic application.

The CV of bisfullerene complex **5** exhibits six well-separated, reversible, one-electron redox waves at −1.25, −1.32, −1.66, −1.82, −2.35, and −2.58 V within the solvent window, as shown in Figure 5. Redox waves of **5** correspond to sequential, pairwise addition of six electrons into the two C_{60} moieties to form C_{60}−Ir_4−C_{60}^{-}, C_{60}^{-}−Ir_4−C_{60}^{-}, C_{60}^{-}−Ir_4−C_{60}^{2-}, ..., and ultimately C_{60}^{3-}−Ir_4−C_{60}^{3-} (vide infra). All three pairs of redox waves are shifted to more negative potentials (190 and 260; 230 and 390; 440 and 670 mV) compared to those of the corresponding free C_{60}. The first redox wave in each pair of the CV is ascribed to reduction of the μ-η^2:η^2-C_{60} ligand because the other μ_4-η^1:η^1:η^2:η^2-C_{60} ligand bonded to four metal atoms and even phosphine-coordinated metal atoms would certainly experience a higher degree of metal-to-C_{60} π-back-donation. Overall, the redox waves of **5** are shifted to more negative potentials relative to those of the related bisfullerene complex $Rh_6(CO)_5(dppm)_2(CNCH_2Ph)(\mu_3$-$\eta^2$:$\eta^2$:$\eta^2$-$C_{60})_2$ (**9**)[11] (−1.19, −1.38, −1.62, −1.86, −2.12, and −2.41 V) due to the stronger metal-to-C_{60} π-back-bonding in **5**. The second redox wave in each pair in the CV of **5** becomes increasingly separated from the first wave (Δ ($E_{1/2}^1$, $E_{1/2}^2$) = 0.07 V, Δ ($E_{1/2}^3$, $E_{1/2}^4$) = 0.16 V, Δ ($E_{1/2}$,^{5} $E_{1/2}^6$) = 0.23 V) as the reduction proceeds. Similar behavior was observed for **9** (Δ ($E_{1/2}^1$, $E_{1/2}^2$) = 0.19 V, Δ ($E_{1/2}^3$, $E_{1/2}^4$) = 0.24 V, Δ ($E_{1/2}$,^{5} $E_{1/2}^6$) = 0.29 V), in which the larger separations are proposed to stem from an increasing Coulombic repulsion between the two C_{60} moieties.[11] This larger increase in the separation within the redox pairs of **9**, however, cannot be explained solely by stronger Coulombic repulsion because the distance between the two C_{60} units in **5** (d(C2−C3′) = 3.23 Å; d(C3−C2′) = 3.25 Å) is shorter than that (ca. 3.56 Å) in **9**. Furthermore, only small redox pair separation is observed for compounds, such as $C_{120}O$[14] and $C_{120}Si(C_6H_5)_2$,[16] with much shorter interfullerene distances of ∼1.5 Å ($C_{120}O$: Δ ($E_{1/2}^1$, $E_{1/2}^2$) = 0.039 V; Δ ($E_{1/2}^3$, $E_{1/2}^4$) = 0.061 V; Δ ($E_{1/2}$,^{5} $E_{1/2}^6$) = 0.138 V;[14] $C_{120}(SiPh_2)$: Δ ($E_{1/2}^1$, $E_{1/2}^2$) = 0.09 V; Δ ($E_{1/2}^3$, $E_{1/2}^4$) = 0.08 V; Δ ($E_{1/2}$,^{5} $E_{1/2}^6$) = 0.14 V[16]). For comparison, separations between stepwise reduction pairs of various organic and inorganic bisfullerenes reported to date are summarized in Table 5 which clearly indicate remarkably efficient electronic com-

(38) Park, J. T.; Cho, J.-J.; Song, H.; Jun, C.-S.; Son, Y.; Kwak, J. *Inorg. Chem.* **1997**, *36*, 2698−2699.
(39) *PeakFit*, Version 4.11; Jandel Scientific Software: San Rafael, CA.

Table 5. Separations (mV) between Stepwise Reduction Pairs of Various Organic and Inorganic Bisfullerenes

compound	$\Delta(E_{1/2}^1, E_{1/2}^2)$	$\Delta(E_{1/2}^3, E_{1/2}^4)$	$\Delta(E_{1/2}^5, E_{1/2}^6)$	solvent	ref
C_{120}	80			DCB	12
$C_{120}C$	80	96	172	DCB	13
$C_{120}O$	39	61	138	DCB	14
$C_{120}(CH_2)_2$	70	75	90	DCB	15
$C_{120}SiPh_2$	90	80	140	DCB	16
$Mo(\eta^2-C_{60})_2(CO)_2$(dbcbipy)	70	80		DCM	21
5	70	160	230	CB	23
9	190	240	290	CB	11

Table 6. Energies and Contributions of Component Parts for Selected MOs for **3** and **6** in CB Solvent

orbital no.	orbital energy (eV)	C_{60} character (%)	cluster character (%)
	3		
LUMO+3	−2.92	46	54
LUMO+2	−3.41	91	9
LUMO+1	−3.49	89	11
LUMO	−3.68	97	3
HOMO	−4.80	36	64
	6		
LUMO+3	−3.47	68	32
LUMO+2	−3.48	91	9
LUMO+1	−3.71	43	57
LUMO	−3.77	92	8
HOMO	−5.02	40	60

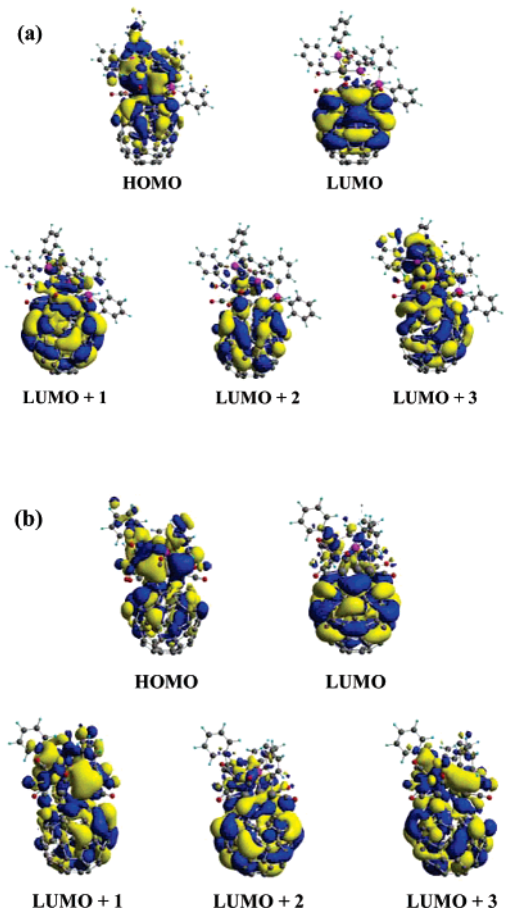

Figure 6. MO diagrams for (a) **3** and (b) **6**.

munication between C_{60} cages through metal cluster spacers in bisfullerenes such as **5** and **9**, in contrast to the other organic and monometallic bisfullerenes.

Theoretical Calculations of 3, 5, and 6. Theoretical studies on C_{60}−metal cluster complexes are very scarce. We have previously performed calculations on triosmium[40] and hexarhodium systems,[11b] while others have done so for the $Ru_3(CO)_9(\mu_3\text{-}\eta^2\text{:}\eta^2\text{:}\eta^2\text{-}C_{60})$ complex.[41] Previous theoretical reports, except for the triosmium system, were limited to a MO analysis of neutral complexes without considering the changes of geometry and electronic structures caused by successive reductions. In the present work, DFT using the BPW91[42] functional was employed to investigate the MOs of **5** and both neutral and anionic species of **3** and **6** in CB solvent, in an effort to understand electrochemical properties observed in the CVs of these complexes. Furthermore, the MPA[43] and HPA[44] were performed to obtain the charge distributions for **3**, **6**, and their anions in CB solvent.

Table 6 lists orbital energies and contributions of C_{60} and metal cluster parts for selected MOs of monofullerene complexes, **3** and **6**, in CB solvent. The corresponding MO diagrams for **3** and **6** are displayed in Figure 6. Highest occupied molecular orbitals (HOMOs) for **3** and **6** are largely metal cluster-based (64% for **3**, and 60% for **6**) with significant C_{60} contributions (36% for **3**, and 40% for **6**), which implies a strong ground-state interaction between C_{60} and Ir_4 cluster centers. Similar ground-state interactions were previously reported for hexarhodium clusters such as $Rh_6(CO)_9(dppm)_2(\mu_3\text{-}\eta^2\text{:}\eta^2\text{:}\eta^2\text{-}C_{60})$ and $Rh_6(CO)_7(dppm)_2(CNCH_2Ph)_2(\mu_3\text{-}\eta^2\text{:}\eta^2\text{:}\eta^2\text{-}C_{60})$.[11b] Energies of lowest unoccupied MOs (LUMOs) of **6** are generally lower than those of **3**, which explains that all the reduction potentials of **6** are shifted to more positive potentials than those of **3** and proves the weaker donor effect of the diphosphine ligand in **6** in comparison with the triphosphine ligand in **3**.

Assuming that added electrons sequentially fill the unoccupied molecular orbitals, LUMO and LUMO+1 orbitals of **3** are responsible for the first and second one-electron and for the third and fourth one-electron reduction steps observed in the CV of **3**, respectively. LUMO+1 of **3** is C_{60}-based (89%), but the metal cluster contribution is not negligible (11%), namely, the electron density in $\mathbf{3}^{3-}$ is delocalized on the metal cluster center. This fact is clearly indicated by the charge increments for $\mathbf{3}^{2-} \rightarrow \mathbf{3}^{3-}$, average values of $\Delta Q(2-/3-) = 37\%$ for C_{60} and 63% for the metal cluster, as shown in Table 7. This explains a large anodic shift of the fourth redox wave of **3**, which essentially overlapped with the third one-electron redox wave at −2.11 V. On the other hand, the LUMO and LUMO+1 orbitals of **6** are responsible for the first one-electron and for

(40) Kim, K. H.; Jung, J.; Han, Y.-K. *Organometallics* **2004**, *23*, 3865−3869.
(41) Lynn, M. A.; Lichtenverger, D. L. *J. Cluster Sci.* **2000**, *11*, 169−188.
(42) (a) Becke, A. D. *Phys. Rev. A* **1988**, *38*, 3098−3100. (b) Perdew, J. P.; Wang, Y. *Phys. Rev. B* **1992**, *45*, 13244−13249.
(43) Mulliken, R. S. *J. Chem. Phys.* **1955**, *23*, 1833−1840.
(44) Hirshfeld, F. L. *Theor. Chim. Acta* **1977**, *44*, 129−138.

Table 7. Charges and Charge Increments of C_{60} and Cluster Parts for **3** and **6** in CB Solvent

		MPA		HPA	
	total charge	C_{60}	cluster	C_{60}	cluster
		3			
Q	0	−0.25	0.25	−0.32	0.32
	−1	−0.98	−0.02	−1.05	0.05
	−2	−1.71	−0.29	−1.79	−0.21
	−3	−2.10	−0.90	−2.13	−0.87
	−4	−2.59	−1.41	−2.61	−1.39
ΔQ	0/−1	0.73	0.27	0.73	0.27
	−1/−2	0.73	0.27	0.74	0.26
	−2/−3	0.39	0.61	0.34	0.66
	−3/−4	0.49	0.51	0.48	0.52
		6			
Q	0	−0.21	0.21	−0.32	0.32
	−1	−0.85	−0.15	−0.97	−0.03
	−2	−1.07	−0.93	−1.12	−0.88
	−3	−1.64	−1.36	−1.70	−1.30
	−4	−2.29	−1.71	−2.38	−1.62
ΔQ	0/−1	0.64	0.36	0.65	0.35
	−1/−2	0.22	0.78	0.15	0.85
	−2/−3	0.57	0.43	0.58	0.42
	−3/−4	0.65	0.35	0.68	0.32

the second one-electron steps observed in the CV of **6**, respectively, since the energy difference between the LUMO and LUMO+1 orbitals is very small (0.06 eV) in this complex. The metal cluster contribution to the LUMO+1 orbital of **6** is large (57%), which implies that the electron density in $\mathbf{6}^{2-}$ is significantly delocalized on the metal cluster center. This is also clearly shown by the charge increments for $\mathbf{6}^{-} \rightarrow \mathbf{6}^{2-}$, average values of $\Delta Q(1-/2-) = 19\%$ for C_{60} and 81% for the metal cluster (see Table 7). These theoretical results are consistent with the observation in the CV of **6** that the second (−1.46 V) and the third (−1.54 V) redox waves are very close to each other and the fourth wave, accordingly, reveals a large anodic shift (230 mV) compared to that of **3**.

To confirm the electronic structures of **3** and **6** in the reduction processes unambiguously, HOMOs of their anions were also investigated and presented in Figure 7. The HOMOs of $\mathbf{3}^{-}$ and $\mathbf{3}^{2-}$ show that the first and second reductions are mainly localized on the C_{60} ligand. The HOMO of $\mathbf{3}^{3-}$ indicates that the electron density in $\mathbf{3}^{3-}$ is somewhat delocalized on the metal cluster part, while the HOMO of $\mathbf{3}^{4-}$ is exclusively localized on the C_{60} cage as well. The HOMO of $\mathbf{6}^{-}$ is also C_{60}-based, but the metal cluster contribution is much larger than that of $\mathbf{3}^{-}$. More electron density in $\mathbf{6}^{-}$ is delocalized on the metal cluster center as compared to $\mathbf{3}^{-}$, which serves to explain the anodic shift of the second wave for **6** (−1.46 V) compared to that of **3** (−1.53 V). Furthermore, the shape of HOMO of $\mathbf{6}^{2-}$ reveals that the electron density in $\mathbf{6}^{2-}$ is significantly delocalized on the metal cluster part, but HOMOs of $\mathbf{6}^{3-}$ and $\mathbf{6}^{4-}$ are again exclusively localized on the C_{60} part. These orbital analyses for anions of **3** and **6** clearly support that reduction processes usually undergo through the C_{60} moiety and the two overlapped or close redox waves in **3** or **6** are correlated with the electron delocalization from the C_{60} unit to the metal cluster moiety.

Theoretical studies of **5** in CB solvent have been similarly carried out to address details of its electrochemical properties shown in Figure 5. MO energies and contributions of metal cluster and two C_{60} parts for selected MOs are listed in Table 8, and MO diagrams are depicted in Figure 8. The HOMO for

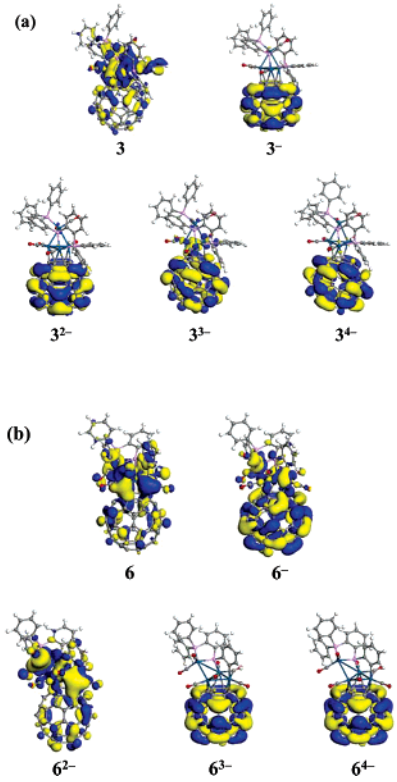

Figure 7. HOMO diagrams for (a) **3** and its anions and (b) **6** and its anions.

Table 8. Orbital Energies and Contributions of C_{60} and Cluster Parts for Selected Molecular Orbitals of **5** in CB Solvent

		C_{60} character (%)		
orbital no.	orbital energy (eV)	C_{60} (left)	C_{60} (right)	cluster character (%)
LUMO+5	−3.24	69	7	24
LUMO+4	−3.27	31	61	8
LUMO+3	−3.28	68	27	5
LUMO+2	−3.43	1	88	11
LUMO+1	−3.52	67	31	2
LUMO	−3.59	26	71	3
HOMO	−4.54	33	18	49

5 is metal cluster-based (49%) with two significant C_{60} contributions (33% (left) and 18% (right)), as similarly observed for $Rh_6(CO)_5(dppm)_2(CNCH_2Ph)(\mu_3\text{-}\eta^2\text{:}\eta^2\text{:}\eta^2\text{-}C_{60})_2$.[11b] The LUMO is C_{60}(right)-based (71%), which evidently indicates that the first reduction is ascribed to the $\mu\text{-}\eta^2\text{:}\eta^2\text{-}C_{60}$ moiety. This theoretical result confirms that the $\mu\text{-}\eta^2\text{:}\eta^2\text{-}C_{60}$ moiety is more electropositive than the $\mu_4\text{-}\eta^1\text{:}\eta^1\text{:}\eta^2\text{:}\eta^2\text{-}C_{60}$ moiety due to less metal-to-C_{60} back-donation in the $\mu\text{-}\eta^2\text{:}\eta^2\text{-}C_{60}$ moiety. Furthermore, LUMO contributions from the two C_{60} units alternate from LUMO to LUMO+5, which explains the alternating electron additions to the two C_{60} units in the six successive reductions, as observed in the CV of **5**. Metal cluster contributions to the MOs are not negligible, up to 24% for LUMO+5, suggesting that the electronic information of one C_{60} ligand is efficiently communicated through the metal cluster spacer to the other C_{60} ligand. The spin-pairing energies apparently exceed the energy gaps (0.01−0.15 eV) among LUMOs of **5**. The metal cluster contribution to LUMOs overall increases as the reduction proceeds, which could be related to the increase in the separation within the redox pairs [Δ ($E_{1/2}^1$, $E_{1/2}^2$) = 0.07 V, Δ ($E_{1/2}^3$, $E_{1/2}^4$) = 0.16 V, Δ ($E_{1/2}$,^{5} $E_{1/2}^6$) = 0.23 V] in the CV of **5**.

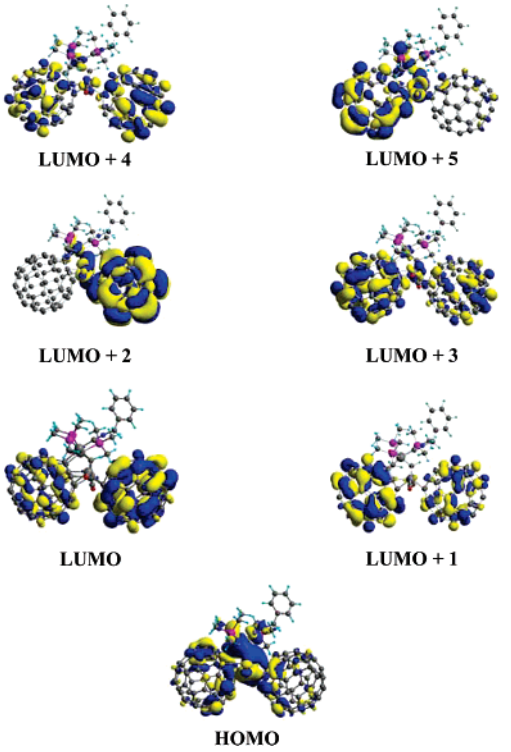

Figure 8. MO diagrams for **5**.

Concluding Remarks

In conclusion, we have found remarkable phosphine conversion: **1**(phosphine) → **2**(diphosphine) → **3**(triphosphine). We have also demonstrated that facile ortho-phosphorylation and ortho-metalation reactions can take place on a tetrairidium framework during the conversion of **1** → **2** → **3** and, more importantly, that the multifunctional C_{60} ligand can assist the ortho-phosphorylation step in the conversion of **2** → **3**. In addition, we have prepared a square planar C_{60}−tetrairidium cluster sandwich complex **5** with two metal centers bridging two C_{60} units, which contains an unprecedented μ_4-η^1:η^1:η^2:η^2-C_{60} bonding mode and an unusual face-capping μ_4-CH moiety. Electrochemical studies, charge population analyses, and DFT MO calculation of **3**, **5**, **6**, and their anions nicely match and clearly allow for the electrochemical pathways of C_{60}−tetrairidium cluster complexes to be understood in detail. In particular, compound **5** reveals an enhanced electronic communication through a wide channel of two metal centers for efficient electronic interactions between C_{60} cages. This work explicitly proves that the electrochemical properties of C_{60}−Ir_4 cluster complexes can be controlled by changing attached ligands on the metal cluster center. These new discoveries may lead to future electronic nanomaterials applications with complexes of this class.

Experimental Section

General Comments. All reactions were carried out under a nitrogen atmosphere with use of standard Schlenk techniques. Solvents were dried over the appropriate drying agents and distilled immediately before use. C_{60} (99.5%, SES Research), $Ir_4(CO)_{12}$ (98%, Strem), PPh_3 (99%, Aldrich), KOH (85%, Junsei), PMe_3 (97%, Aldrich), deutrated-PMe_3 (99+atom %D, Aldrich), and benzylisocyanide (98%, Aldrich) were used without further purification. $Ir_4(CO)_9(PPh_3)_3$,[45] $Ir_4(CO)_9(PMe_3)_3$,[46] $Ir_4(CO)_9(PEt_3)_3$,[46] $Ir_4(CO)_8(PMe_3)_4$,[46] $Ir_4(CO)_8(P(CD_3)_3)_4$,[46] $Ir_4(CO)_8(dppm)_2$,[47] and **6**[22] were prepared by the literature methods. Preparative thin layer plates were prepared with silica gel GF_{254} (Type 60, E. Merck). Infrared spectra were obtained on a Bruker EQUINOX-55 FT-IR spectrophotometer. ^{1}H(400 MHz) and ^{13}C(100 MHz) NMR spectra were recorded on a Bruker AVANCE-400 spectrometer and ^{31}P(122 MHz) NMR spectra on a Bruker AM-300 spectrometer. Positive-ion FAB mass spectra (FAB^+) were obtained by the staff of the Korea Basic Science Institute (KBSI), and all *m*/*z* values are referenced to ^{193}Ir. Elemental analyses were performed by the staff of the Energy & Environment Research Center at KAIST.

Preparation of 2. A CB solution (30 mL) of **1** (50 mg, 0.028 mmol) was heated to reflux for 40 min. Evaporation of the solvent and purification by preparative TLC (CH_2Cl_2/C_6H_{14} = 1:1) produced **2** (29.6 mg, 0.018 mmol, 64%, R_f = 0.8) as an orange solid: IR(C_6H_{12}): ν_{CO} 2062 (w), 2049 (s), 2029 (vs), 2011 (vs), 1993 (vs), 1956 (m), 1946 (m) cm^{-1}; ^{1}H NMR (400 MHz, $CDCl_3$, 298 K): δ 8.44 (dd, 1H, J_{PH} = 8.0 Hz, J_{PH} = 2.5 Hz), 7.89 (m, 1H), 7.63(m, 4H), 7.46−6.88 (m, 24H), 6.62 (m, 2H), 6.51 (t, 1H, J_{PH} = 7.6 Hz) (all C_6H_5 + C_6H_4); ^{13}C NMR (100 MHz, $CDCl_3$, 298 K): δ 186.8 (s, 1CO), 185.7 (s, 1CO), 179.6 (s, 1CO), 176.4 (s, 1CO), 166.4 (s, 1CO), 165.7 (s, 1CO), 165.5 (d, 1CO, $^2J_{CP}$ = 3.5 Hz), 163.7 (d, 1CO, $^2J_{CP}$ = 4 Hz), 153.2−124.3 (42C, C_6H_5 + C_6H_4); ^{31}P{H} NMR (122 MHz, $CDCl_3$, 298 K): δ 24.2 (d, 1P, $^2J_{PP}$ = 22.1 Hz), 16.4 (s, 1P), −42.9 (d, 1P, $^2J_{PP}$ = 22.1 Hz); MS (FAB^+): *m*/*z*: 1624 [M^+]. Anal. Calcd for $C_{50}H_{33}Ir_4O_8P_3$: C, 36.99; H, 2.05. Found: C, 36.76; H, 2.19.

Preparation of 3. A CB solution (30 mL) of **1** (30 mg, 0.017 mmol) and C_{60} (2 equiv, 24 mg, 0.033 mmol) was heated to reflux for 3 h. Evaporation of the solvent and purification by preparative TLC (CS_2/CH_2Cl_2 = 8:1) produced compound **3** (13.2 mg, 0.006 mmol, 36%, R_f = 0.7) as a greenish-black solid: IR(CH_2Cl_2): ν_{CO} 2045 (vs), 2016 (vs), 1998 (s), 1985 (sh), 1970 (m) cm^{-1}; ^{1}H NMR (400 MHz, $CDCl_3$, 298K): δ 8.07−7.14 (m, 24H), 6.93−6.78 (m, 3H) (all C_6H_4 + C_6H_4); ^{13}C NMR (100 MHz, $C_6D_4Cl_2$, 298K): δ 188.4 (d, 1CO, J_{PC} = 2.5 Hz), 187.3 (d, 1CO, J_{PC} = 3.2 Hz), 179.9 (s, 1CO), 173.3 (t, 1CO, J_{PC} = 3.9 Hz), 172.4 (d, 1CO, J_{PC} = 12.2 Hz), 161.2(dd, 1CO, J_{PC} = 51.2 Hz, J_{PC} = 5.5 Hz), 158.9−143.6 (54C, C_{60} sp^2 region), 79.1 (d, 1C, J_{PC} = 6.3 Hz, C_{60} sp^3 π-bonded carbon) 68.0 (t, 1C, J_{PC} = 4.9 Hz, C_{60} sp^3 π-bonded carbon), 64.1 (d, 1C, J_{PC} = 2.4 Hz, C_{60} sp^3 π-bonded carbon), 62.7 (s, 1C, C_{60} sp^3 π−bonded carbon), 61.2 (d, 1C, J_{PC} = 4.5 Hz, C_{60} sp^3 π-bonded carbon), 60.6 (dd, 1C, J_{PC} = 13.8 Hz, J_{PC} = 2.3 Hz, C_{60} sp^3 π-bonded carbon); ^{31}P{H} NMR (122 MHz, CS_2/ext. CD_2Cl_2, 298K): δ 31.2 (d, 1P, $^2J_{PP}$ = 12.8 Hz), −16.3 (dd, 1P, $^2J_{PP}$ = 12.8 Hz, $^2J_{PP}$ = 4.0 Hz), −21.5 (d, 1P, $^2J_{PP}$ = 4.0 Hz); MS (FAB^+): *m*/*z*: 2210 [M^+]. Anal. Calcd for $C_{102}H_{27}Ir_4O_6P_3$: C, 55.43; H, 1.23. Found: C, 55.64; H, 1.42.

Conversion of 2 to 3. A CB solution (30 mL) of **2** (30 mg, 0.018 mmol) and C_{60} (2 equiv, 26 mg, 0.036 mmol) was heated to reflux for 3 h. Evaporation of the solvent and purification by preparative TLC (CS_2/CH_2Cl_2 = 8:1) afforded compound **3** (15.1 mg, 0.007 mmol, 41%, R_f = 0.7) as a greenish-black solid.

Preparation of 5 and 5d. A DCB solution (30 mL) of **4** (30 mg, 0.023 mmol) and C_{60} (67 mg, 0.093 mmol, 4 equiv) was prepared in a 100 mL Schlenk flask equipped with a reflux condenser, and the solution was heated to reflux for 2 h. The reaction mixture was purified by preparative TLC to give a green band (CS_2/CH_2Cl_2 = 4:1, R_f = 0.35), which was dissolved in CB (50 mL). Benzyl isocyanide (2.0 mg, 0.0038 mmol) in 0.25 mL of CB was added to the green solution of the green band via a syringe, and the resulting solution was stirred at 70 °C for 2 h. Solvent removal under vacuum and purification by preparative TLC (CS_2/CH_2Cl_2 = 2:1) gave **5** (8 mg, 0.0023 mmol, 13%) as a dark green solid. IR(CH_2Cl_2) ν_{CN} 2159 (w) cm^{-1}; ν_{CO} 1986 (s)

(45) Drakesmith, A. J.; Whyman, R. *J. Chem. Soc., Dalton Trans.* **1973**, 362−367.
(46) (a) Darensbourg, D. J.; Baldwin-Zuschke, B. J. *Inorg. Chem.* **1981**, *20*, 3846−3850. (b) Darensbourg, D. J.; Baldwin-Zuschke, B. J. *J. Am. Chem. Soc.* **1982**, *104*, 3906−3910.
(47) Ros, R.; Scrivanti, A.; Albano, V. G.; Braga, D.; Garlaschelli, L. *J. Chem. Soc., Dalton Trans.* **1986**, 2411−2421.

Table 9. Crystallographic Data for **2**, **3**, and **5**

	2	**3**	**5**
formula	$C_{50}H_{33}P_3O_8Ir_4$	$C_{102}H_{27}P_3O_6Ir_4 \cdot 4CS_2$	$C_{140}H_{32}NO_3P_3Ir_4 \cdot C_6H_4Cl_2 \cdot 1.75CS_2$
fw	1623.47	2514.47	2917.60
cryst syst	triclinic	monoclinic	monoclinic
space group	$P\bar{1}$	$P2_1/c$	$P2_1/n$
a, Å	11.087(1)	17.472(5)	18.139(2)
b, Å	11.472(1)	20.071(6)	24.386(3)
c, Å	21.576(2)	22.639(6)	22.478(3)
α, deg	91.925(2)	90	90
β, deg	101.719(2),	100.739(5)	110.283(2)
γ, deg	116.070(1)	90	90
V, Å^3	2390.1(4)	7800(4)	9327(2)
Z	2	4	4
D_{calcd}, g cm^{-3}	2.256	2.141	2.078
temp, K	293(2)	293(2)	173(2)
λ(Mo Kα), Å	0.71073	0.71073	0.71073
μ, mm^{-1}	11.254	7.144	5.948
θ range for collection	$1.95° < \theta < 28.02°$	$1.69° < \theta < 25.52°$	$1.25° < \theta < 28.28°$
no. of rflns measd	14 826	40 827	53 694
no. of unique rflns	10 924	14 530	21 663
R_{int}	0.0394	0.0716	0.0748
GOF	1.044	0.953	1.034
R1[a]	0.0576	0.0422	0.0646
wR2[b]	0.1476	0.0859	0.1528

[a] $R1 = \sum||F_o| - |F_c||/\sum |F_o|$. [b] $wR2 = [\sum\omega(F_o^2 - F_c^2)^2/\sum\omega(F_o^2)^2]^{1/2}$.

cm^{-1}; ^{1}H NMR (1,2-$C_6D_4Cl_2$, 298K) δ 15.52 (d, 1H, J_{PH} = 13.0 Hz, μ_4-C*H*), 7.66−7.20 (m, 5H, CNCH$_2$C$_6$*H*$_5$), 5.18 (AB pattern, 2H, J = 16.5 Hz, CNC*H*$_2$C$_6$H$_5$), 3.55 (d, 3H, J_{PH} = 7.0 Hz, C*H*$_3$-μ-P−CH$_3$), 3.04 (d, 3H, J_{PH} = 4.6 Hz, CH$_3$-μ-P−C*H*$_3$), 2.07 (d, 9H, J_{PH} = 9.8 Hz, P*Me*$_3$), 1.86 (d, 9H, J_{PH} = 9.1 Hz, P*Me*$_3$); ^{31}P{^{1}H} NMR (1,2-$C_6D_4Cl_2$, 298 K) δ 164.3 (s, 1P, μ-*P*Me$_2$), −44.9 (s, 1P, *P*Me$_3$), −47.9 (s, 1P, *P*Me$_3$); Anal. Calcd for $C_{147}H_{32}O_3NP_3Ir_4$: C, 63.75; H, 1.22; N, 0.53. Found: C, 63.40; H, 1.59; N, 0.81.

A similar treatment of $Ir_4(CO)_8(P(CD_3)_3)_4$ to **5** gave a deuterium-labeled analogue, **5d**: ^{1}H NMR (1,2-$C_6D_4Cl_2$, 298K) δ 7.66−7.20 (m, 5H, CNCH$_2$C$_6$*H*$_5$), 5.18 (AB pattern, 2H, J = 16.5 Hz, CNC*H*$_2$C$_6$H$_5$); ^{31}P{^{1}H} NMR (1,2-$C_6D_4Cl_2$, 298 K) δ 163.4 (s, 1P, μ-*P*(CD$_3$)$_2$), −46.6 (s, 1P, *P*(CD$_3$)$_3$), −49.6 (s, 1P, *P*(CD$_3$)$_3$).

X-ray Crystallographic Studies. Crystals of **2**, **3**, and **5** suitable for an X-ray analysis were grown by slow solvent diffusion: for **2** with methanol into dichloromethane at room temperature, for **3** with heptane into carbon disulfide at room temperature, and for **5** with methanol into carbon disulfide/DCB (1:1) at room temperature. Diffraction data of **2** and **3** were collected on a Siemens SMART diffractometer/CCD area detector at room temperature. Diffraction data of **5** were collected on a Bruker SMART diffractometer/CCD area detector at 173 K. Preliminary orientation matrix and cell constants were determined from three series of ω scans at different starting angles. The hemisphere of reflection data was collected at scan intervals of 0.3° ω with an exposure time of 10 s per frame. The data were corrected for Lorentz and polarization effects, but no correction for crystal decay was applied. Absorption corrections were performed using SADABS.[48]

Each structure was solved by direct[49] and difference Fourier methods and was refined by full-matrix least-squares methods based on F^2 (SHELX 97).[50] All non-hydrogen atoms were refined with anisotropic thermal coefficients. Details of relevant crystallographic data for **2**, **3**, and **5** are summarized in Table 9.

Electrochemical Measurements. Cyclic voltammetry was carried out on a AUTOLAB (PGSTAT 10, Eco Chemie, Netherlands) electrochemical analyzer using the conventional three-electrode system of a platinum working electrode (1.6 mm diameter disk, Bioanalytical Systems, Inc.), a platinum counter wire electrode (5 cm length of 0.5 mm diameter wire), and a Ag/Ag$^+$ reference electrode (0.1 M $AgNO_3$/Ag in acetonitrile with a Vycor salt bridge). All measurements were performed at ambient temperature under nitrogen atmosphere in a dry, deoxygenated 0.1 M CB solution of [(*n*-Bu)$_4$N]ClO$_4$. The concentrations of compounds were ca. 3×10^{-4} M. All potentials were referenced to the standard ferrocene/ferrocenium (Fc/Fc$^+$) scale. The relative number of electrons involved in each reduction process was obtained from the graph of current vs (time)$^{-1/2}$ according to the Cottrell equation.[51]

Computational Details. Our calculations were based on the DFT at the generalized gradient approximation (GGA) level (Becke's 1988 functional for exchange and Perdew-Wang's 1991 functional for correlation, BPW91[42]). The energy-consistent relativistic effective core potential (RECP) was used for Ir atoms.[52] Double numerical plus polarization (DNP) basis sets were used for the C, H, O, N, and P atoms, and the VEs for Ir were also expanded using the DNP basis set. All the structures of **3**, **5**, and **6** were optimized without any symmetry restriction using the analytical gradients of the energies. We have performed the MPA[43] and the HPA[44] for **3**, **6**, and their anions in order to obtain the charge distributions. The geometry optimization and the population analysis were performed using the DMol3 software.[53]

The MOs for **3**, **5**, and **6** were calculated at the optimized structures using the Gaussian03 software package.[54] The energy-consistent RECP with corresponding basis sets[52] was used for the Ir atoms, and 6-31G(d) basis sets were used for the other atoms. Solvation energies were calculated using the conductor-like screening model (COSMO)[55] to consider bulk solvent effects effectively. The dielectric constant value (ϵ = 5.6) of CB was employed in the COSMO calculations.

Acknowledgment. This work was supported by the Korea Research Foundation Grant funded by the Korean Government (MOEHRD) (KRF-2005-201-C00021) and by the Nano R&D

(48) Sheldrick, G. M. *SADABS, A program for area detector absorption corrections*; University of Göttingen: Göttingen, Germany, 1994.
(49) Sheldrick, G. M. *Acta Crystallogr. A* **1990**, *46*, 467−473.
(50) Sheldrick, G. M. *SHELX97, Program for Crystal Structure Refinement*; University of Göttingen: Göttingen, Germany, 1997.
(51) Bard, A. J.; Faulkner, L. R. *Electrochemical Methods*; John Wiley and Sons: New York, 1980; pp 142−146.
(52) Andrae, D.; Häussermann, U.; Dolg, M.; Stoll, H.; Preuss, H. *Theor. Chim. Acta* **1990**, *77*, 123−141.
(53) (a) Delley, B. *J. Chem. Phys.* 1990, *92*, 508−517. (b) Delley, B. *J. Chem. Phys.* **1991**, *94*, 7245−7250. (c) Delley, B. *J. Phys. Chem.* **1996**, *100*, 6107−6110. (d) Delley, B. *J. Chem. Phys.* **2000**, *113*, 7756−7764.
(54) Frisch, M. J., et al. *Gaussian 03*, Revision C.02; Gaussian, Inc.; Wallingford, CT, 2004.
(55) Klamt, A.; Schüürmann, G. *J. Chem. Soc., Perkin Trans. 2* **1993**, 799−805.

program (2005-02618) of the Korea Science and Engineering Foundation (KOSEF) funded by Korean Ministry of Science & Technology (MOST). This work was also supported in part by the SRC program (R11-2005-008-03001-0) of the KOSEF through the Center for Intelligent Nano-Bio Materials at Ewha Womans University.

Supporting Information Available: Details of the crystallographic studies of **2**, **3**, and **5** (PDF); X-ray crystallographic files for **2**, **3**, and **5** (CIF); and complete ref 54. This material is available free of charge via the Internet at http://pubs.acs.org.

JA0616027